

Cover Page



Universiteit Leiden



The handle <http://hdl.handle.net/1887/20311> holds various files of this Leiden University dissertation.

Author: Vallés Pardo, José Luis

Title: In *silico* study of reaction mechanisms and design principles for water oxidation catalysts

Date: 2012-12-19

***In silico* study of reaction mechanisms
and design principles for water oxidation
catalysts**

José Luis Vallés Pardo

José Luis Vallés Pardo

In silico study of reaction mechanisms and design principles for water oxidation catalysts

Ph.D. Thesis, Leiden University, December 2012

No part of this thesis may be reproduced in any form without the express written permission of the copyright holders.

***In silico* study of reaction mechanisms and design principles for water oxidation catalysts**

PROEFSCHRIFT

ter verkrijging van de graad van Doctor aan de Universiteit Leiden,
op gezag van Rector Magnificus Prof. Mr. P.F. van der Heijden,
volgens besluit van het College voor Promoties
te verdedigen op woensdag 19 december 2012
klokke 8.45 uur

door

José Luis Vallés Pardo

geboren te València, Spanje in 1985

Promotiecommissie

Promotor:

Prof. Dr. Huub J.M. de Groot

Copromotor:

Dr. Francesco Buda

Overige leden:

Prof. Dr. Jaap Brouwer

Prof. Dr. Marc van Hemert

Prof. Dr. Jürg Hutter

Prof. Dr. Marc Koper

The use of supercomputer facilities was sponsored by The Netherlands National Computing Facilities Foundation (NCF), with financial support from the Netherlands Organization for Scientific Research (NWO). This research is financed in part by the BioSolar Cells open innovation consortium, supported by the Dutch Ministry of Economic Affairs, Agriculture and Innovation (project C1.9).

Table of contents

List of abbreviations	9
Notation	11
Preface	13
Chapter 1: Introduction.....	15
1.1 Natural and artificial photosynthesis	17
1.1.1 Photosystem II	17
1.1.2 Oxygen Evolving Complex	19
1.1.3 Artificial photosynthesis	20
1.2 Water oxidation catalysts (WOC).....	21
1.3 Aim and scope of this thesis	24
1.4 Bibliography	27
Chapter 2: Theoretical methods.....	31
2.1 Introduction	33
2.2 Born-Oppenheimer Approximation.....	33
2.3 Density Functional Theory	36
2.4 Exchange-Correlation functionals	38
2.5 Gaussian-plane waves method.....	40
2.6 Molecular Dynamics.....	42
2.6.1 Car-Parrinello Molecular Dynamics.....	43
2.6.2 Born-Oppenheimer Molecular Dynamics.....	45
2.6.3 Metadynamics.....	46
2.7 Bibliography	48

Chapter 3: Structural rearrangements and reaction intermediates in a di-Mn water oxidation catalyst.....	51
3.1 Introduction	53
3.2 Computational details	55
3.3 Results and discussion	58
3.3.1 Modeling of the Hexa-coordinated complex with two oxo-bridges (1).....	58
3.3.1.1 Structural and electronic characterization	58
3.3.1.2 Reaction pathway analysis for complex 1	61
3.3.2 Modeling of the penta-coordinated manganese cluster (2) with one oxo-bridge.....	65
3.3.2.1 Structural and electronic characterization of complex 2.....	65
3.3.2.2 Reaction pathway analysis for complex	68
3.4 Conclusions	72
3.5 Bibliography	75
Chapter 4: Ab-initio molecular dynamics study of water oxidation reaction pathways in mono-Ru catalysts.....	79
4.1 Introduction	81
4.2 Computational details	83
4.3 Results and discussion	86
4.3.1 Characterization of the $[(Ar)Ru(O)(bpy)]^{+2}$	86

4.3.2 AIMD simulations for the O-O bond formation.....	90
4.3.2.1 Ru-Ow3 approach.....	92
4.3.2.2 Ox-Ow1 approach.....	94
4.3.3 Characterization of the [(benzene)Ru(OOH)(bpy)] ⁺¹ intermediate and the transition state.....	98
4.4 Conclusions	102
4.5 Bibliography	104
Chapter 5: In silico prediction and thermodynamic study of novel mono-nuclear water oxidation catalysts.....	107
5.1 Introduction	109
5.2 Methodology and computational details.....	113
5.3 Results and discussion	118
5.3.1. Influence of the aromatic ligand.....	120
5.3.2. Influence of the metallic center	123
5.4 Conclusions	126
5.5 Bibliography	129
Chapter 6: General Discussion and Outlook	133
Summaries	137
Curriculum Vitae	153
List of Publications	155
Nawoord	157

List of abbreviations

ADF	Amsterdam Density Functional program
AIMD	Ab-initio molecular dynamics
B3LYP	Becke 3-Parameter, Lee-Yang-Parr exchange-correlation functional
BLYP	Becke-Lee-Yang-Parr exchange-correlation functional
BOMD	Born-Oppenheimer Molecular Dynamics
CHARMM	Chemistry at HARvard Molecular Mechanics force field
CMD	Constrained molecular dynamics
Cp	Cyclopentadienyl
Cp*	Pentamethylcyclopentadienyl
CP2K	Open Source Molecular Dynamics software package
CPMD	Car-Parrinello Molecular Dynamics
CV	Collective Variable
DFT	Density functional theory
DZVP	Double Zeta Valence Plus basis set with one set of Polarization functions
EXAFS	Extended X-ray absorption fine structure
FES	Free-energy surface
GGA	Generalized Gradient Approximation
GPW	Gaussian and plane waves method
GTH	Goedecker-Teter-Hutter pseudopotential
GTO	Gaussian type orbitals
KS	Kohn-Sham
LDA	Local Density Approximation
MD	Molecular Dynamics
MM	Molecular Mechanics
MTD	Metadynamics
OEC	Oxygen evolving complex
OPBE	Perdew-Burke-Ernzerhof exchange-correlation functional
PBC	Periodic Boundary Conditions
PCET	Proton-Coupled Electron Transfer
PSII	Photosystem II

PWs	Plane Waves
QM	Quantum Mechanics
QM/MM	Quantum Mechanics/Molecular Mechanics
QS	QuickStep
TZP	Triple-Zeta basis set with one set of Polarization functions
TZVP	Triple Zeta Valence Plus basis set with one set of Polarization functions
WOR	Water oxidation reaction

Notation

\hat{A}	Operator A
χ, χ_s	Response function
χ_μ	Basis set function
χ_p	Primitive basis function
Δ	Laplacian
∇	Nabla
ϵ_0	Permittivity of vacuum
e	Electron charge, exponent
E	Energy
E_{xc}	Exchange-correlation functional
\hbar	Planck constant
\hat{H}	Hamiltonian
J	Coulomb electron-electron repulsion
m	Electron mass
M	Nuclear mass
n	In a summation, the number of electrons
N	In a summation, the number of nuclei
Ψ	Wavefunction of a system
ϕ	Kohn-Sham orbital
ρ	Electron density
\mathbf{r}	Vector position of electrons in space.

\mathbf{r}_i	Position of electron i
r_{ij}	Distance between electrons i and j
\mathbf{R}	Position of the nuclei
\mathbf{R}_I	Position of nucleus I
R_{IJ}	Distance between nuclei I and J
$\dot{\mathbf{R}}$	First time derivative of \mathbf{R}
$\ddot{\mathbf{R}}$	Second time derivative of \mathbf{R}
t	Time
T	Kinetic energy
V	Potential energy
Z	Atomic number
E_{eff}	Effective potential
v_{ext}	External potential
$P_{\mu\nu}$	Density matrix
Ω	Volume of the unit cell
\mathbf{G}	Reciprocal lattice vectors
$s(x)$	Collective variable
h	Height of the bias potential
w	Width of the bias potential
τ_g^{-1}	Deposition rate of the bias potential

Preface

Fossil fuel is among the most important valuables for the developed and the developing world. Since the industrial revolution its use and demand has been growing exponentially, arriving to the point where limitations to its availability can be expected within less than three decades, in the most optimistic analyses.

Even more worrying than this possible lack of primary energy supply are the environmental consequences of society moved by carbon-based fuels. The biosphere is not able to assimilate the vast amount of CO₂ released into the atmosphere by burning fuel.

For these reasons a transition to carbon-free or carbon-neutral primary energy carriers is urgent. What could be the best solution? Probably there is not a universal solution. It is not a competition for the best, first or quickest scientific development. The society has a problem and the scientific community should do its best in order to solve it.

In this framework one interesting direction is the development of an efficient device to perform the water splitting process in order to use hydrogen as a clean fuel, an “artificial leaf”, by which the conversion of solar energy into chemical energy on a large scale may become reality.

Chapter 1:

Introduction

1.1 Natural and artificial photosynthesis

Photosynthesis is the physical-chemical process by which plants, algae and some bacteria convert the solar energy into chemical energy, through the synthesis of organic compounds. In these organisms, the photosynthetic processes lead to the release of molecular oxygen and the removal of carbon dioxide from the atmosphere that is used to synthesize carbohydrates. Photosynthesis provides the energy and reduced carbon required for the survival of virtually all life on our planet, as well as the molecular oxygen necessary for the survival of oxygen consuming organisms [1-3].

1.1.1 Photosystem II

Photosystem II (PSII) is a multi-subunit protein complex embedded in the thylakoid membranes of higher plants, algae and cyanobacteria. It uses solar energy to catalyze a series of electron transfer reactions resulting in the splitting of water into molecular oxygen, protons and electrons. These reactions dissipate power on a scale of ~100 TW, being responsible for the production of atmospheric oxygen and indirectly for almost all the biomass on the planet [4].

Despite its importance, the catalytic properties of PSII have never been reproduced in any artificial system. Understanding its unique chemistry is not only important in its own right, but could have implications for the development of systems that allow us to obtain a clean source of chemical energy, reproducing the natural reaction.

The photosystem II complex is composed of more than fifteen polypeptides and at least nine different redox components that have been shown to undergo light-induced electron transfer [5]. However, only five of these redox components are known to be involved in transferring electrons from H₂O to the plastoquinone pool, and one of them is the water oxidizing tetra-manganese cluster from the oxygen evolving complex (OEC).

Photosystem II is the only known protein complex that can oxidize water, resulting in the release of molecular oxygen into the atmosphere. Despite years of research, the molecular events that lead to water oxidation are still a matter of current investigations. Energetically, water is a poor electron donor. The oxidation-reduction midpoint potential of water is +0.82 V (pH 7). In photosystem II this reaction is driven by the oxidized chlorophyll *a* in the reaction center, P680⁺, which has a midpoint potential estimated to be +1.2 V at pH 7). Water oxidation requires two molecules of water and involves four sequential turnovers of the reaction centre. This was shown by an experiment demonstrating that oxygen release by photosystem II occurs with a four flash dependence [6, 7]. Each photochemical reaction creates an

oxidant that removes one electron from the system, resulting in a net reaction that involves the release of one oxygen molecule, the deposition of four protons into the inner water phase, and the transfer of four electrons to the Q_B -site, producing two reduced plastoquinone molecules [8-10].

1.1.2 Oxygen Evolving Complex

The photosynthetic oxygen evolution occurs at a specialized site of PSII called the oxygen-evolving complex (OEC) [5, 11]. To couple the single-electron photochemistry of the PSII reaction centre to the four-electron oxidation of two water molecules to molecular oxygen, the OEC cycles through five intermediate states, denoted S_i , where the index i indicates the number of positive charges accumulated at the OEC and runs from 0 to 4. The S_4 state decays spontaneously back to the S_0 state, releasing an oxygen molecule. The catalytic centre of the OEC is a Mn_3O_4Ca cubane with a fourth manganese atom outside the cube. The detailed structure of the OEC has been matter of debate during the last decade, with the most accepted structures being the Ferreira and the Loll model [12, 13]. However, more recently a higher resolution structure has been obtained from X-Ray data by Umena et al. [14]. Moreover, there is increasing converging evidence that the four oxidizing equivalents are not accumulated, instead they are used throughout the S-state cycle to extract electrons and protons from two

water molecules bound to the MnCa cluster in the S_0 state. In addition, it is known that calcium and chloride ions are required to perform the water-oxidation catalysis and it is thought that their location is close to the MnCa cluster [5].

The radical states formed during the reaction on the substrate water intermediates are stabilized by increasing the oxidation state of the MnCa cluster. During each step of the S_0 - S_4 cycle one proton and one electron are released, the system remains electroneutral, and no coulombic restriction is imposed to the system by the increase of the oxidation state of the manganese atoms. However, there is considerable discussion about the mechanistic details of this reaction [15-17].

1.1.3 Artificial photosynthesis

The aim of the artificial photosynthesis research is to obtain an “artificial leaf”, a device able to perform the same hydrolysis reaction as in the natural system in order to obtain hydrogen using water as the raw material.

This device needs to have different modules to mimic and perform the various stages of the photochemistry as in the photosynthetic organisms. An antenna system is needed for efficient light harvesting. A charge separator complex is crucial to stabilize the radicals formed upon photoinduced electron transfer and to delay the charge recombination. A robust and efficient catalyst is also necessary to

perform the water oxidation cycle. Moreover, the complete device, the artificial leaf, must be self-healing in order to reduce the possible light damage along the whole process [18].

During the last two decades, important scientific progress has been obtained in the field of light harvesting units and charge separation systems [19-21]. However, one of the bottlenecks in artificial photosynthetic research is the chemical design of a synthetic water splitting catalyst able to perform the multi electron oxidation reaction at high turnover number and frequency, with moderate overpotential and high current density.

1.2 Water oxidation catalysts (WOC)

The natural PSII system has been the inspiration and the starting point for many researchers in developing a catalytic structure for efficient water oxidation. The search of a molecular catalyst capable to generate oxygen from the oxidation of two water molecules has been very active already in the eighties and nineties with the study and synthesis of several biomimetic catalysts, mainly with two manganese centres linked by oxygen bridges [22-25]. Also ruthenium has been used extensively as metallic centre in similar catalyst architectures [25, 26].

During the last decade a large effort has been devoted in the synthesis of catalysts with different kind and number of metallic centres and different ligands [27]. The most explored catalysts are the ones based on ruthenium [28, 29], cobalt [30-32] and iridium [33-35], and during the last years also iron has been explored as a possible metallic centre [36]. DFT calculations have been also performed to clarify the underlying reaction mechanism in some of these catalysts [34, 35, 37-39]. Available computational chemistry tools have reached a predictive power which is good enough to allow not only the understanding of reaction mechanisms in existing catalysts, but even the important and crucial landmark of assisting in the design of new catalysts.

An effective water oxidation catalyst must be capable of water oxidation at a potential minimally above the thermodynamic value, with a high turnover frequency and able to run during hundred thousands of cycles. However, these are characteristics needed only from an efficiency point of view. For a good catalyst it is also necessary to use an abundant material. A catalyst based on a rare and expensive metal might represent a problem when moving into a large scale production.

Nowadays, the catalysts with the best performance are based on ruthenium or iridium. However, these two metals are extremely rare, leading to an economical and availability problem. This is the reason why the search for other catalysts based on more abundant metals has been a hot topic during the last years. In Figure 1.1 it is possible to

Introduction

observe that ruthenium is around four orders of magnitude less abundant than cobalt, and six to eight orders of magnitude less abundant than manganese and iron, respectively. Iridium is still less abundant than ruthenium. At this point is clear that a compromise between efficiency and availability is crucial in order to find the most appropriate catalysts for the water oxidation reaction.

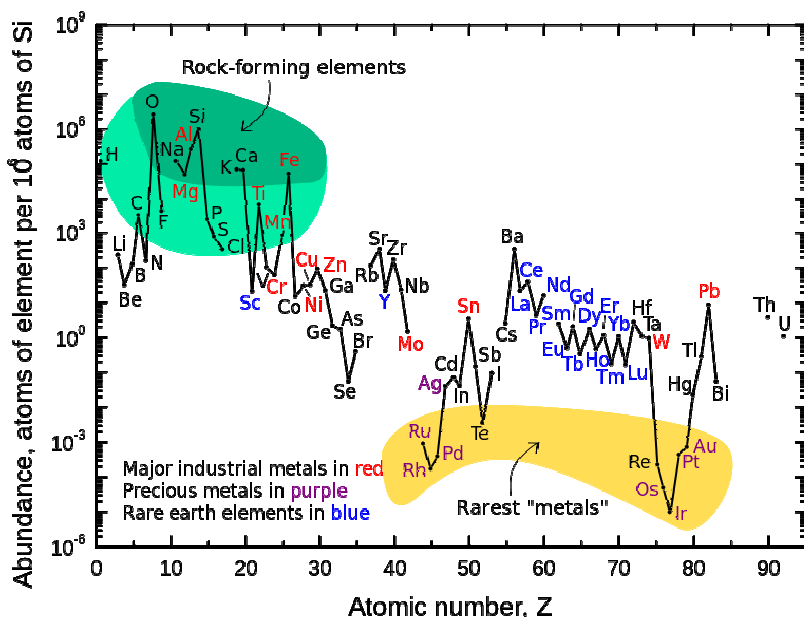


Figure 1.1. Relative abundance of elements in the Earth's upper crust. Not shown: Noble Gases, Tc(43), Pm(61), and all elements after Bi(83), except for Th(90) and U(92).

1.3 Aim and scope of this thesis

Throughout the last decades the water oxidation process has been extensively investigated. However, open questions remain on the reaction mechanism and the possible intermediates in the catalytic cycle. Indeed, different catalysts can function through different reaction routes. Some of them work in a proton-coupled electron transfer (PCET) pathway, while other catalysts have a non-PCET behaviour.

Some of these problems lie in the very short lifetime of intermediates, which makes it difficult to characterize them experimentally. Within this context, DFT calculations represent a very useful tool. In fact quantum-mechanical computational tools allow exploring and analyzing the possible intermediates and study and compare different reaction pathways in order to find the energetically most likely one. In the same way the thermodynamics of the catalytic cycle and the kinetics of the reaction coordinates can be analyzed.

The specific aim of this thesis is the study of different catalysts and reaction pathways to find clues about the mechanism of the reaction and develop guiding principles for the design of efficient water oxidation complexes.

Chapter 2 gives a general overview of the theoretical methods and approximations used throughout this thesis. In chapter 3 a mechanistic

study of one of the first Mn based catalysts, the $[\text{H}_2\text{O}(\text{terpy})\text{Mn}(\text{O})_2\text{Mn}(\text{terpy})\text{OH}_2]^{3+}$ complex, is presented. The novelty of this work is the use of *ab initio* molecular dynamics simulations tools to include dynamics and explicit solvent effects. Moreover, methods used to simulate rare events are here employed to explore the reaction pathway and allow crossing the activation energy barrier within the typical *ab initio* molecular dynamics time scale. A structural rearrangement and a new intermediate complex are found which can explain degradation processes observed in experimental work. In chapter 4, the mechanism for the oxygen-oxygen bond formation of mono-nuclear ruthenium based catalysts is studied with computational tools based on DFT similarly to those used in the previous chapter. One important finding in this work is that the explicit inclusion of the water environment is crucial to properly characterize the reaction pathway. Indeed the solvent is not a simple spectator but participates in the reaction as proton acceptor to facilitate the formation of the intermediate hydroperoxo complex and to perform the complete oxygen bond formation reaction. Thereafter, in chapter 5, the thermodynamics of the complete S_0 - S_4 cycle is analyzed and compared for mono-metallic catalysts of the same family as the one analyzed in chapter 4. Here we modify *in silico* the metallic centre and the aromatic ring ligand to explore their effect on the thermodynamic cycle and on the resulting overpotential. This work aims to identify important common denominators and guiding principles in the design of water

oxidation catalysts. Finally, in chapter **6**, a general overview of the main conclusions obtained in this thesis is given. In this chapter is also presented a brief introduction to the current and future research, as well the new techniques that can be put into practice to improve the understanding of this catalytic reaction.

1.4 Bibliography

1. Amesz, J., *Photosynthesis*, Elsevier, Amsterdam, **1987**.
2. Cramer, W.A., Knaff, D.B., *Energy transduction in Biological Membranes*, Springer, Berlin, **1991**.
3. Govindjee, *Photosynthesis*, Academic Press, New York, **1982**.
4. Hermann, W.A., *Energy*, 31 (**2006**) 1685-1702.
5. Debus, R.J., *Biochimica et Biophysica Acta (BBA) - Bioenergetics*, 1102 (**1992**) 269-352.
6. Govindjee, *Bioenergetics of Photosynthesis*, Academic Press, New York, **1975**.
7. Joliot, P., Barbieri, G., Chabaud, R., *Photochemistry and Photobiology*, 10 (**1969**) 309-329.
8. Renger, G., *Photosynthesis Research*, 38 (**1993**) 229-247.
9. Klein, M., Sauer, K., Yachandra, V., *Photosynthesis Research*, 38 (**1993**) 265-277.
10. Lavergne, J., Junge, W., *Photosynthesis Research*, 38 (**1993**) 279-296.
11. Rutherford, A.W., Zimmermann, J.L., Boussac, A., *The Photosystems: Structure, Function and Molecular Biology*, Elsevier, Amsterdam, **1992**.
12. Ferreira, K.N., Iverson, T.M., Maghlaoui, K., Barber, J., Iwata, S., *Science (New York, N.Y.)*, 303 (**2004**) 1831-1838.
13. Loll, B., Kern, J., Saenger, W., Zouni, A., Biesiadka, J., *Nature*, 438 (**2005**) 1040-1044.
14. Umena, Y., Kawakami, K., Shen, J.-R., Kamiya, N., *Nature*, 473 (**2011**) 55-60.
15. Hoganson, C.W., Babcock, G.T., *Science*, 277 (**1997**) 1953-1956.
16. Tommos, C., Babcock, G.T., *Biochimica et Biophysica Acta (BBA) - Bioenergetics*, 1458 (**2000**) 199-219.

17. Dau, H., Haumann, M., *Biochimica et biophysica acta*, 1767 (2007) 472-483.
18. Nocera, D.G., *Accounts of Chemical Research*, 45 (2012) 767-776.
19. Wasielewski, M.R., *Accounts of Chemical Research*, 42 (2009) 1910-1921.
20. Albinsson, B., Martensson, J., *Journal of Photochemistry and Photobiology C: Photochemistry Reviews*, 9 (2008) 138-155.
21. Benniston, A.C., Harriman, A., *Materials Today*, 11 (2008) 26-34.
22. Calvin, M., *Science*, 184 (1974) 375-381.
23. Limburg, J., Vrettos, J.S., Liable-Sands, L.M., Rheingold, A.L., Crabtree, R.H., Brudvig, G.W., *Science*, 283 (1999) 1524-1527.
24. Siegbahn, P.E., *Inorganic chemistry*, 39 (2000) 2923-2935.
25. Yagi, M., Kaneko, M., *Chemical Reviews*, 101 (2000) 21-36.
26. Rüttinger, W., Dismukes, G.C., *Chemical Reviews*, 97 (1997) 1-24.
27. Liu, X., Wang, F., *Coordination Chemistry Reviews*, 256 (2012) 1115-1136.
28. Xu, Y., Akermark, T., Gyollai, V., Zou, D., Eriksson, L., Duan, L., Zhang, R., Akermark, B., Sun, L., *Inorganic Chemistry*, 48 (2009) 2717-2719.
29. Wasylenko, D.J., Ganesamoorthy, C., Koivisto, B.D., Henderson, M.A., Berlinguette, C.P., *Inorganic Chemistry*, 49 (2010) 2202-2209.
30. Kanan, M.W., Nocera, D.G., *Science*, 321 (2008) 1072-1075.
31. Jiao, F., Frei, H., *Angewandte Chemie International Edition*, 48 (2009) 1841-1844.
32. Yin, Q., Tan, J.M., Besson, C., Geletii, Y.V., Musaev, D.G., Kuznetsov, A.E., Luo, Z., Hardcastle, K.I., Hill, C.L., *Science (New York, N.Y.)*, 328 (2010) 342-345.
33. McDaniel, N.D., Coughlin, F.J., Tinker, L.L., Bernhard, S., *Journal of the American Chemical Society*, 130 (2007) 210-217.

34. Hull, J.F., Balcells, D., Blakemore, J.D., Incarvito, C.D., Eisenstein, O., Brudvig, G.W., Crabtree, R.H., *Journal of the American Chemical Society*, 131 (2009) 8730-8731.
35. Blakemore, J.D., Schley, N.D., Balcells, D., Hull, J.F., Olack, G.W., Incarvito, C.D., Eisenstein, O., Brudvig, G.W., Crabtree, R.H., *Journal of the American Chemical Society*, 132 (2010) 16017-16029.
36. Ertem, M.Z., Gagliardi, L., Cramer, C.J., *Chemical Science*, 3 (2012) 1293-1299.
37. Polyansky, D.E., Muckerman, J.T., Rochford, J., Zong, R., Thummel, R.P., Fujita, E., *Journal of the American Chemical Society*, 133 (2011) 14649-14665.
38. Wang, L.-P., Wu, Q., Van Voorhis, T., *Inorganic Chemistry*, 49 (2010) 4543-4553.
39. Wang, T., Brudvig, G.W., Batista, V.S., *Journal of chemical theory and computation*, 6 (2010) 2395-2401.

Chapter 2:

Theoretical Methods

2.1 Introduction

In this chapter a brief description of the theoretical methods and approximations used in this thesis is presented. In the first place, the Born-Oppenheimer approximation will be summarized, followed by a short introduction to Density Functional Theory and a discussion on the exchange-correlation functionals. Finally an overview of the *ab-initio* molecular dynamics theory will be given, together with the recent implementation of the metadynamics approach for describing events that are rare on the time scale of molecular dynamics simulations.

2.2 Born-Oppenheimer Approximation

The time-dependent Schrödinger equation,

$$\hat{H} \Psi(\mathbf{r}, \mathbf{R}, t) = i\hbar \frac{\partial \Psi(\mathbf{r}, \mathbf{R}, t)}{\partial t}, \quad (2.1)$$

is a non-relativistic description of the system and it is only valid when the velocity of the particles is small in comparison with the speed of light. Since \hat{H} is not time dependent for the molecular complexes of interest in this thesis, the equation **2.1** can be simplified to the time-independent Schrödinger equation

$$\hat{H}\Psi(\mathbf{r}, \mathbf{R}) = E\Psi(\mathbf{r}, \mathbf{R}). \quad (2.2)$$

Following the Born interpretation of the wavefunction, Ψ has to satisfy the normalization condition [1]

$$\langle \Psi | \Psi \rangle = 1. \quad (2.3)$$

The Hamiltonian contains kinetic and potential energy terms and can be written as

$$\begin{aligned} \hat{H} = & \hat{T}_N(\mathbf{R}) + \hat{T}_e(\mathbf{r}) + \hat{V}_{N-N}(\mathbf{R}) \\ & + \hat{V}_{e-e}(\mathbf{r}) + \hat{V}_{e-N}(\mathbf{r}, \mathbf{R}) \end{aligned} \quad (2.4)$$

where $\hat{T}_N(\mathbf{R})$ is the kinetic energy operator for the nuclei,

$$\hat{T}_N = -\frac{\hbar^2}{2} \sum_I^N \frac{1}{M_I} \left(\frac{\partial^2}{\partial X_I^2} + \frac{\partial^2}{\partial Y_I^2} + \frac{\partial^2}{\partial Z_I^2} \right), \quad (2.5)$$

and $\hat{T}_e(\mathbf{r})$ is the electronic kinetic energy operator

$$\hat{T}_e = -\frac{\hbar^2}{2} \sum_i^n \frac{1}{m} \left(\frac{\partial^2}{\partial x_i^2} + \frac{\partial^2}{\partial y_i^2} + \frac{\partial^2}{\partial z_i^2} \right). \quad (2.6)$$

The potential energy part consists of the nuclear-nuclear repulsion, the electron-electron repulsion and the electron-nuclear attraction, written respectively as

$$\hat{V}_{N-N} = \frac{1}{4\pi\epsilon_0} \sum_I^N \sum_{J>I}^N \frac{Z_I Z_J e^2}{R_{IJ}}, \quad (2.7)$$

$$\hat{V}_{e-e} = \frac{1}{4\pi\epsilon_0} \sum_i^n \sum_{j>i}^n \frac{e^2}{r_{ij}} \quad (2.8)$$

and

$$\hat{V}_{e-N} = -\frac{1}{4\pi\epsilon_0} \sum_i^n \sum_l^N \frac{Z_l e^2}{r_{il}}. \quad (2.9)$$

Since the mass of the nuclei is much larger than the mass of the electrons, it can be assumed to a good approximation that the electronic distribution in a system depends only on the positions of the nuclei and not on their velocities. In the Born-Oppenheimer approximation this physical fact is used to separate the Schrödinger equation into an equation for the electronic wavefunction and one for the nuclear wavefunction. The electronic Schrödinger equation is written as

$$\hat{H}_e \Psi_e(\mathbf{r}; \mathbf{R}) = E_{\text{eff}}(\mathbf{R}) \Psi_e(\mathbf{r}; \mathbf{R}), \quad (2.10)$$

where the electronic Hamiltonian \hat{H}_e is

$$\hat{H}_e = \hat{T}_e(\mathbf{r}) + \hat{V}_{e-e}(\mathbf{r}) + \hat{V}_{e-N}(\mathbf{r}, \mathbf{R}) + \hat{V}_{N-N}(\mathbf{R}) \quad (2.11)$$

and the electronic wavefunction $\Psi_e(\mathbf{r}; \mathbf{R})$, as well as the electronic energy $E_{\text{eff}}(\mathbf{R})$, depend only parametrically on the nuclear positions which are considered fixed.

The electronic energy $E_{\text{eff}}(\mathbf{R})$ plays the role of an effective potential in the nuclear Schrödinger equation,

$$\hat{H}_N \chi_N = (\hat{T}_N(\mathbf{R}) + E_{\text{eff}}(\mathbf{R}))\chi_N, \quad (2.12)$$

and is usually called the potential energy surface (PES).

2.3 Density Functional Theory

As the wave function for an N -electron system is a function of $3N$ independent spatial variables, solving the electronic Schrödinger equation (2.10) using traditional *ab-initio* quantum chemistry approaches, such as configuration interaction (CI), becomes computationally very demanding for large molecular complexes. Density functional theory (DFT) offers a valuable alternative that is computationally more efficient than *ab-initio* methods and yet is quite accurate. This theory is based on the Hohenberg-Kohn theorem [2] showing that it is possible to use just the electronic density to calculate the ground-state energy E_0 . Hence the complexity of the problem decreases drastically, since the electronic density is a function of only three coordinates, and is independent of the number of electrons. Given an external potential $v_{\text{ext}}(\mathbf{r})$, the total electronic energy can be expressed as a functional of the electron density $\rho(\mathbf{r})$,

$$E \equiv E_v[\rho(\mathbf{r})] \equiv \int v_{\text{ext}}(\mathbf{r})\rho(\mathbf{r})d\mathbf{r} + F[\rho(\mathbf{r})], \quad (2.13)$$

where $F[\rho(\mathbf{r})]$ is an universal functional and the integral runs over the entire space. For molecular systems the external potential $v_{\text{ext}}(\mathbf{r})$ is usually the potential generated by the nuclei (see equation 2.9).

The Hohenberg-Kohn theorem also proves that a variational principle for the energy functional holds: For any density, the energy given by the corresponding energy functional is never smaller than the ground-state energy, and the ground-state energy is obtained only using the exact ground-state electron density.

The total energy functional can be written as a sum of different terms:

$$E_v[\rho] = T[\rho] + V_{e-N}[\rho] + V_{e-e}[\rho], \quad (2.14)$$

where $T[\rho]$ is the electronic kinetic energy, $V_{e-N}[\rho]$ is the energy due to the electron-nuclear attraction, and $V_{e-e}[\rho]$ is the electron-electron repulsion energy, which can be decomposed into classical Coulomb and non-classical contributions:

$$V_{e-e}[\rho] = J[\rho] + V_{e-e}^{\text{nc}}[\rho]. \quad (2.15)$$

While $V_{e-N}[\rho]$ and $J[\rho]$ can be calculated in terms of the electron density as

$$V_{e-N}[\rho] = \int v_{\text{ext}}(\mathbf{r})\rho(\mathbf{r})d\mathbf{r} \quad (2.16)$$

and

$$J[\rho] = \int \frac{\rho(\mathbf{r})\rho(\mathbf{r}')}{|\mathbf{r} - \mathbf{r}'|} d\mathbf{r}d\mathbf{r}', \quad (2.17)$$

the explicit form for the kinetic energy functional and the non-classical electron-electron repulsion energy are unknown. In order to simplify the calculations of the kinetic energy term, Kohn and Sham proposed to compute $T_s[\rho]$, which is the kinetic energy for a set of independent particles. This term can be easily written in terms of a set of orbitals, known as the Kohn-Sham orbitals. The remaining unknown part of the kinetic energy $T_c[\rho]$ is the kinetic correlation energy, which leads to

$$T[\rho] = T_c[\rho] + T_s[\rho]. \quad (2.18)$$

The $T_c[\rho]$ contribution of the kinetic energy is then combined with the non-classical electron-electron repulsion term in the exchange-correlation functional,

$$E_{xc}[\rho] = T_c[\rho] + V_{ee}^{nc}[\rho], \quad (2.19)$$

and the energy functional can be rewritten as

$$E_v[\rho] = T_s[\rho] + V_{e-N}[\rho] + J[\rho] + E_{xc}[\rho]. \quad (2.20)$$

2.4 Exchange-Correlation functionals

The exact form of the exchange-correlation functional is unknown and therefore the main approximation in DFT is in the treatment of this

functional. One of the first proposed approximations is the local density approximation (LDA) in which the system is treated locally as a uniform electron gas using

$$E_{xc}^{\text{LDA}}[\rho] = \int e_{xc}(\rho(\mathbf{r}))\rho(\mathbf{r})d\mathbf{r}, \quad (2.21)$$

where the exchange-correlation energy function $e_{xc}(\rho)$ has been calculated with high accuracy from quantum Monte Carlo for the homogeneous electron gas [3]. The LDA approximation turned out to work well for metals and semiconductors [4]. However, it performs poorly for molecules, especially in predicting binding energies. This is no surprise since the electron density in molecular systems is highly inhomogeneous. To improve the exchange-correlation functional also the knowledge of the gradient of the density is included in the generalized gradient approximation (GGA):

$$E_{xc}^{\text{GGA}}[\rho, \nabla\rho] = \int f(\rho(\mathbf{r}), \nabla\rho(\mathbf{r}))d\mathbf{r}. \quad (2.22)$$

More recently a new generation of functionals, the meta-GGA functionals, have been proposed including also the Laplacian of the density [5, 6]:

$$E_{xc}^{\text{mGGA}}[\rho, \nabla\rho, \nabla^2\rho] = \int f(\rho(\mathbf{r}), \nabla\rho(\mathbf{r}), \nabla^2\rho(\mathbf{r}))d\mathbf{r}. \quad (2.23)$$

The GGA functionals that are mostly used in this thesis are the BLYP, which combines the exchange functional of Becke with the correlation functional of Lee, Yang and Parr [7, 8], and the OPBE, which combines the OPTx exchange with the PBE correlation part [9]. The choice of the OPBE functional is justified by previous work where it has been shown to give an accurate description for transition metal complexes [10, 11].

Other functionals that are broadly used are the hybrid functionals. In these functionals part of the exact Hartree-Fock exchange energy is mixed with the GGA functional, according to

$$E_{xc}^{\text{hybrid}}[\rho] = E_{xc}^{\text{GGA}}[\rho, \nabla\rho] + c_x \left(E_x^{\text{HF}}[\rho] - E_x^{\text{GGA}}[\rho] \right) \quad (2.24)$$

The c_x parameter determines the mixing between the Hartree-Fock and GGA exchange. Two hybrid functionals used in this thesis are the B3LYP and B3LYP*, which differ in the amount of exact exchange, 20% for B3LYP and 15% in B3LYP* [10].

2.5 Gaussian-plane waves method

The expression for the total electronic energy in the Kohn-Sham formulation of DFT is shown in equation 2.22. Within the Gaussian-plane waves (GPW) approach [11] the electronic density ρ is defined

by two different representations. The first one is based on a set of atom centred contracted Gaussian functions with the density matrix $P_{\mu\nu}$:

$$\rho(\mathbf{r}) = \sum_{\mu=1, \nu=1}^K P_{\mu\nu} \varphi_{\mu}(\mathbf{r}) \varphi_{\nu}(\mathbf{r}), \quad (2.25)$$

where K is the total number of contracted Gaussian basis functions, φ_{μ} , defined as

$$\varphi_{\mu}(\mathbf{r}) = \sum_{m=1}^M C_{m\mu} g_m(\mathbf{r}), \quad (2.26)$$

in which $g_m(\mathbf{r})$ are the M primitive Gaussian functions used in the linear combination. The introduction of atomic pseudopotentials removes the core electrons from the calculation.

In order to evaluate the density dependent terms, $J[\rho]$ and $E_{xc}[\rho]$, the second representation is used, in which the density is expanded in an auxiliary set of plane waves:

$$\tilde{\rho}(\mathbf{r}) = \frac{1}{\Omega} \sum_{\mathbf{G}}^{\mathbf{G}_{\max}} \tilde{\rho}(\mathbf{G}) e^{i\mathbf{G}\cdot\mathbf{r}}, \quad (2.27)$$

where the sum over the \mathbf{G} vectors extends up to a maximum value, \mathbf{G}_{\max} , which depends on the plane waves energy cutoff, and Ω is the volume of the cell.

The expansion coefficients $\tilde{\rho}(\mathbf{G})$ are such that $\tilde{\rho}(\mathbf{r})$ is equal to $\rho(\mathbf{r})$ on a regular grid in the unit cell. The difference $|\rho(\mathbf{r}) - \tilde{\rho}(\mathbf{r})|$ goes to zero as the energy cutoff goes to infinity.

Using this dual representation the KS energy expression [2, 12], showed in equation 2.22, within the GPW framework is defined as

$$\begin{aligned}
 E(\rho) = & \sum_{\mu\nu}^K P_{\mu\nu} \left\langle \varphi_{\mu}(\mathbf{r}) \left| -\frac{1}{2} \nabla^2 \right| \varphi_{\nu}(\mathbf{r}) \right\rangle \\
 & + \sum_{\mu\nu}^K P_{\mu\nu} \left\langle \varphi_{\mu}(\mathbf{r}) \left| V_{\text{loc}}^{\text{PP}}(\mathbf{r}) \right| \varphi_{\nu}(\mathbf{r}) \right\rangle \\
 & + \sum_{\mu\nu}^K P_{\mu\nu} \left\langle \varphi_{\mu}(\mathbf{r}) \left| V_{\text{nl}}^{\text{PP}}(\mathbf{r}, \mathbf{r}') \right| \varphi_{\nu}(\mathbf{r}') \right\rangle \\
 & + 2\pi\Omega \sum_{\mathbf{G}}^{\text{G max}} \frac{\tilde{\rho}^*(\mathbf{G}) \tilde{\rho}(\mathbf{G})}{\mathbf{G}^2} + E_{\text{xc}}[\rho(\mathbf{r})] + \frac{1}{2} \sum_{I \neq J}^N \frac{Z_I Z_J}{|R_{IJ}|}.
 \end{aligned} \tag{2.28}$$

$V_{\text{e-N}}[\rho]$ is described by norm-conserving pseudopotentials with a potential split in a local part $V_{\text{loc}}^{\text{PP}}(\mathbf{r})$ and a fully non-local part $V_{\text{nl}}^{\text{PP}}(\mathbf{r}, \mathbf{r}')$.

2.6 Molecular Dynamics

Molecular dynamics [13, 14] is a well established method to study thermodynamic properties of complex many-particle systems at finite temperature. The idea is to evolve in time the atoms in the system according to the classical equations of motion to closely match the microscopic evolution of the system. Macroscopic thermodynamic

properties of the system can then be computed based on the ergodic hypothesis that the statistical ensemble averages are equal to time averages along the trajectory of the system.

Similar analyses can be performed with *ab-initio* molecular dynamics, in which the explicit calculation of the electronic structure is used to compute potential energies and forces [15]. A significant advantage of *ab-initio* molecular dynamics is that no parameterization of an empirical potential is needed and that systems can be simulated when unexpected chemical events take place.

In this section a brief overview of two different AIMD methods used in this thesis will be given, the Car-Parrinello Molecular Dynamics, used in the CPMD program [16], and the Born-Oppenheimer Molecular Dynamics, used in the CP2K software package [17].

2.6.1 Car-Parrinello Molecular Dynamics

The main idea of this approach [18] is the treatment of the electronic degrees of freedom, the KS orbitals ψ_i , as fictitious classical dynamical variables, taking advantage of the time scale separation between the fast electronic and slow nuclear motion to avoid energy exchange between them. The Car-Parrinello Lagrangian contains the nuclear kinetic energy, the fictitious electronic kinetic energy and the potential energy

$$\begin{aligned}
L_{\text{CP}} = & \sum_{I=1}^N \frac{1}{2} M_I \dot{\mathbf{R}}_I^2 + \frac{1}{2} \mu \sum_{i=1}^n \int \left| \dot{\psi}_i(\mathbf{r}) \right|^2 d\mathbf{r} \\
& - E_v[\psi_i, \mathbf{R}] + \sum_{i=1, j=1}^n \Lambda_{ij} (\langle \psi_i | \psi_j \rangle - \delta_{ij})
\end{aligned} \tag{2.29}$$

with the orbitals subject to the holonomic constraints of orthonormality. The potential energy, $E_v[\psi_i, \mathbf{R}]$ is given by eq. 2.22. A fictitious mass, μ , is assigned to the electronic degrees of freedom and can be tuned to ensure the adiabaticity.

The Newtonian equations of motion are obtained from the associated Euler-Lagrange equations, and the corresponding Car-Parrinello equations are

$$M_I \ddot{\mathbf{R}}_I = -\nabla_I E_v[\psi, \mathbf{R}] \tag{2.30}$$

and

$$\mu \ddot{\psi}_i = -\frac{\delta E_v}{\delta \langle \psi_i |} + \sum_{j=1}^n \Lambda_{ij} \psi_j. \tag{2.31}$$

These equations can be solved numerically through standard finite difference algorithms used in molecular dynamics, such as the Verlet algorithm [19, 20]. The constant of motion in the Car-Parrinello dynamics is

$$E_{\text{cons}} = \sum_{I=1}^N \frac{1}{2} M_I \dot{\mathbf{R}}_I^2 \tag{2.32}$$

$$+ \frac{1}{2} \sum_{i=1}^n \mu \left\langle \dot{\psi}_i \left| \dot{\psi}_i \right. \right\rangle + E_v[\psi_i, \mathbf{R}]$$

The fictitious electronic mass is chosen in such a way to ensure that the lowest electronic frequency exceeds the highest frequency of the nuclei. In this way energy transfer from the nuclear to the electronic subsystem is avoided at least on the time scale of the AIMD simulations. The choice of the fictitious electronic mass will then also determine the choice of the time step in the numerical algorithm. A typical time step in Car-Parrinello MD simulations is 0.1 fs.

2.6.2 Born-Oppenheimer Molecular Dynamics

An alternative approach for *ab-initio* MD is to solve self-consistently the electronic structure for *each* molecular dynamics step given the set of nuclear positions at that particular instant in time. Thus, the electronic structure part represents the self-consistent solution of the KS equations, if we use DFT for computing the forces on the nuclei. Then these forces are used to propagate only the nuclear positions at the next time step in the classical molecular dynamics. Since in the BOMD approach the electronic degrees of freedom are not propagated in time, the choice of the time step is limited only by the nuclear characteristic frequencies and therefore can be usually 5 to 10 times larger than in CPMD. On the other hand in BOMD the electronic ground state has to be reached in each molecular dynamics step and the efficiency of this approach will strongly depend on the speed of convergence in the self-

consistent loop.

2.6.3 Metadynamics

Ab-initio molecular dynamics methods have been successfully applied during the last decades for different problems from materials science to biochemistry [21]. However, the main limitation of this approach is that it is still limited to processes occurring within a few tens of picoseconds. This will be particularly relevant if one is interested in studying chemical reactions, since these will usually not take place spontaneously on such a short time scale. Typically energy barriers of many kcal/mol need to be overcome. Several strategies have been developed to face this problem and the metadynamics method, introduced by Laio and Parrinello [22], appears to be one of the most efficient and robust solutions. The metadynamics method introduces a biasing potential in a collective variable space that influences the “real” dynamics. The collective variables selected to explore the configuration space of interest can be different parameters: from distances or angles to coordination numbers or the formation of a hydronium. The selection of the appropriate collective variables is a crucial point in obtaining accurate results with this technique.

The biasing potential is built in such a way to disfavour the configurations already visited and to facilitate the exploration of regions of the configuration space that are statistically unlikely. In all the work presented in this thesis the history dependent potential is

constructed as a sum of Gaussians, along distances as collective variables, according to

$$V_G(s(x), t) = \int_0^t d\tau \frac{h}{\tau_g} \exp\left[-\frac{(s(x) - s(x(\tau)))^2}{2w^2}\right], (2.33)$$

where h is the height and w the width of the Gaussian bias potential, and τ_g^{-1} the frequency of deposition.

Moreover, the same bias potentials used to escape from the energy minima, will eventually converge to the free-energy profile, $F(s)$, along the chosen reaction coordinate. Therefore this method not only allows to find reaction pathways, but also to estimate reaction free-energies and activation barriers.

2.7 Bibliography

1. Born, M., Heisenberg, W., Jordan, P., *Zeitschrift für Physik A Hadrons and Nuclei*, 35 (1926) 557-615.
2. Hohenberg, P., Kohn, W., *Physical Review*, 136 (1964) B864-B871.
3. Ceperley, D.M., Alder, B.J., *Physical Review Letters*, 45 (1980) 566-569.
4. Parr, R.G., Yang, W., *Density-Functional Theory of Atoms and Molecules* Oxford University Press, 1989.
5. Zhao, Y., Truhlar, D.G., *The Journal of Chemical Physics*, 125 (2006) 194101.
6. Zhao, Y., Truhlar, D., *Theoretical Chemistry Accounts: Theory, Computation, and Modeling (Theoretica Chimica Acta)*, 120 (2008) 215-241.
7. Becke, A.D., *Physical Review A*, 38 (1988) 3098-3100.
8. Lee, C., Yang, W., Parr, R.G., *Physical Review B*, 37 (1988) 785-789.
9. Swart, M., Ehlers, A.W., Lammertsma, K., *Molecular Physics*, 102 (2004) 2467-2474.
10. Becke, A.D., *The Journal of Chemical Physics*, 98 (1993) 5648-5652.
11. Lippert, G., Parrinello, M., Hutter, J., *Molecular Physics*, 92 (1997) 477-488.
12. Kohn, W., Sham, L.J., *Physical Review*, 140 (1965) A1133-A1138.
13. Allen, M.P., Tildesley, D.J., *Computer simulations of liquids*, Clarendon Press, Oxford, 1987.
14. Frenkel, D., Smit, B., *Understanding molecular simulation*, 2nd ed., Academic Press, 2002.

15. Marx, D., Hutter, J., *Ab initio molecular dynamics: Theory and Implementation*, FZ Jülich, Germany,, **2000**.
16. CPMD, <http://www.cpmc.org/>, Copyright IBM Corp 1990-2011, Copyright MPI für Festkörperforschung Stuttgart 1997-2001
17. The CP2K developers group. <http://cp2k.berlios.de/>.
18. Car, R., Parrinello, M., *Physical Review Letters*, 55 (**1985**) 2471-2474.
19. Verlet, L., *Physical Review*, 159 (**1967**) 98-103.
20. Swope, W.C., Andersen, H.C., Berens, P.H., Wilson, K.R., *The Journal of Chemical Physics*, 76 (**1982**) 637-649.
21. Marx, D., Hutter, J., *Ab Initio Molecular Dynamics: Basic Theory and Advanced Methods*, Cambridge University Press, Cambridge, **2009**.
22. Laio, A., Parrinello, M., *Proceedings of the National Academy of Sciences of the United States of America*, 99 (**2002**) 12562-12566.

This chapter is based on:

J.L. Vallés-Pardo, H.J.M. de Groot and F. Buda, Physical Chemistry Chemical Physics, 14 (2012) 15502-15508.

Chapter 3:

Structural rearrangements and reaction intermediates in a di-Mn water oxidation catalyst

3.1 Introduction

A key process in natural photosynthesis is the four-electron four-proton water oxidation reaction producing O₂. This reaction takes place in the oxygen evolving complex (OEC) of photosystem II (PSII), which consists of a tetramanganese cluster with several oxo-bridges [1]. A mechanistic insight in the water splitting process is fundamental for the development of artificial devices for solar energy storage. High resolution crystallographic, EXAFS and spectroscopic data, combined with computational modeling, mostly based on Density Functional Theory (DFT), have recently provided structural and mechanistic insight in the catalytic cycle taking the OEC through the states S₀ to S₄ [2-6]. In parallel there has been a growing effort in synthesizing biomimetic complexes that could efficiently perform the catalytic O₂ formation from water [7]. An optimal catalyst for water oxidation should properly address various requirements, most noticeably a good efficiency, low cost, and good stability. Man made catalysts are mostly based on Ru, and Co [8-12], and the search for complexes based on more abundant elements, such as Mn or Fe, is progressing [13, 14]. One of the first successful attempts in this direction is the Mn-complex [H₂O(terpy)Mn(O)₂Mn(terpy)OH₂]³⁺ (terpy = 2,2':6,2''-terpyridine), which contains two Mn atoms linked by two μ-oxo bridges [15]. This complex is able to catalyze the formation of O₂ from water, although it

also shows a high degree of deactivation by ligand loss and permanganate formation [16-19].

Since the catalyst is based on Mn and uses more than one metal ion connected by oxo-bridges, in a way similar to the natural OEC, this catalyst has been the subject of extensive theoretical investigations to elucidate the nature of the key intermediates in the catalytic cycle [13, 20, 21]. On the basis of density functional theory (DFT) calculations, it has been suggested that the active species in the O–O bond formation step is the $[(\text{bis}(\text{imino})\text{pyridine})(\text{H}_2\text{O})\text{Mn}^{\text{IV}}(\mu\text{-O})_2\text{Mn}^{\text{V}}(\text{O})(\text{bis}(\text{imino})\text{pyridine})]^{3+}$ complex (**1**) [20]. In a recent work by Nakamura *et al.*, an alternative reaction path for oxygen formation has been proposed based on a direct involvement of excess oxidants acting as counterions, such as OCl^- [22]. Most of the previous theoretical mechanistic studies address hypothetical transition states and intermediates in a static approach and do not include an explicit description of the water solvation.

In this study *ab-initio* molecular dynamics simulations are used with an additional time-dependent bias potential along specific reaction coordinates as proposed by Laio and Parrinello [23]. Both hybrid quantum-mechanics/molecular mechanics (QM/MM) and full QM simulations are employed to include explicitly the solvent environment. In this way several potential reaction paths can be explored including dynamics and solvation effects. The simulations show that the di-Mn cluster can undergo a structural rearrangement and form a complex that

is weakly active in the O-O bond formation. The slow kinetics of this step can allow other processes, including linear degradation of the catalyst, in line with the deactivation processes observed experimentally [16-19]. These results can help to guide the chemical design of molecular scaffolds with specific structural features for the implementation of stable water oxidation catalysts with improved durability.

3.2 Computational details

The *ab-initio* molecular dynamics (AIMD) simulations in this work were performed with the CPMD program [24]. Nuclear forces in AIMD are derived from the electronic structure using DFT with the BLYP functional [25, 26]. The choice of a non-hybrid functional is mostly dictated by computational efficiency in the AIMD. However, single point calculations using the hybrid functionals OPBE0, B3LYP, B3LYP* [27], that differ in the amount of exact exchange (25%, 20% and 15%, respectively), have been performed with the ADF program [28-30] to check the relative energy of different complexes in order to validate the BLYP results. Further tests have been performed with the ADF program to check the effect of empirical dispersion corrections in the form proposed by Grimme [31].

Norm-conserving pseudopotentials of the Martins–Troullier [32] form are used for all the atomic elements except for Mn, for which the Goedecker form is used instead [33]. The Kohn-Sham orbitals are expanded on a plane-waves basis set with an energy cutoff of 100 Ry, which provides a good convergence in relative energies.

The Car-Parrinello AIMD simulations are performed with a time step $\Delta t = 5$ a.u. and a fictitious electronic mass $\mu = 400$ a.u. In order to efficiently explore possible reaction pathways, the CPMD code with the metadynamics approach is used [23]. The metadynamics is a coarse-grained dynamics on the free-energy surface (FES) defined by a few collective variables, such as distances, angles, and coordination numbers. The method uses an adaptive bias potential to escape from local minima. In these simulations the evolution of the collective variables takes one metadynamics step every ten AIMD time steps. At each metadynamics step the evolution of the collective variables is guided by a generalized force that combines the action of the thermodynamic force, which would trap the system in a free energy minimum, and a history-dependent force that disfavors configurations already visited. This history-dependent potential is built as a sum of Gaussian functions centered in the explored values of the collective variables [23]. The width and height of the Gaussian are parameters that can be tuned to find the best compromise between accuracy in the FES estimate and speed in crossing energy barriers to sample the whole collective variable space. In this work these values are 0.1 a.u. and

0.001 Hartree, respectively. In this work metadynamics simulations are used to explore hypothetical reaction paths rather than to accurately estimate free-energy barriers.

For a more realistic study of the reaction the solvent is included explicitly within a QM/MM approach as implemented in the CPMD code [34, 35]. QM/MM simulations are performed in a cubic box containing the di-Mn catalyst and about 1000 water molecules. The di-Mn cluster and a few (3-4) closest water molecules that can play an active role in the reaction are included in the QM subsystem treated at the DFT level, while the remaining water molecules are treated with Molecular Mechanics (MM). For the MM part the AMBER force field is used with the TIP3P model for the water molecules [36]. The solvent environment is equilibrated at room temperature with a classical MD while the Mn complex is kept fixed. In addition, AIMD simulations for complex **2** are performed with a full QM solvent environment with 72 water molecules in a box $20.5 \times 23.8 \times 18.1 \text{ \AA}^3$.

3.3 Results and discussion

3.3.1 Modeling of the Hexa-coordinated complex with two oxo-bridges (1)

3.3.1.1 Structural and electronic characterization

In order to validate the choice of the functional and basis set described in the previous section, the structural and electronic properties of complex **1** obtained with DFT results are compared using a hybrid functional [20]. The geometry of complex **1** is optimized for different multiplicities and report the resulting relevant geometrical parameters and relative energies in Table **3.1** (see also Figure **3.1** for the atomic labelling). The most stable spin state and the order of higher energy multiplicities are consistent with previous DFT results [20]. In particular, the energy difference between the lowest energy doublet and the sextet is found to be 5.6 kcal/mol in BLYP vs. 3.04 kcal/mol in B3LYP. This difference is consistent with the general finding that a non-hybrid functional, like the BLYP, favours the low spin states over the high spin states, contrary to hybrid functionals. In Table **3.1** also the bond lengths obtained in Ref. [20] for the lowest energy (doublet) spin state are reported.

Overall the bond lengths obtained with BLYP are similar to those obtained with B3LYP, the larger difference being found for $d(\text{Mn2-O3})$

which is 0.15 Å shorter in these calculations. As already discussed in Ref.[20], a shorter Mn-oxo ligand distance corresponds with a weaker radical character of the oxygen, which is also confirmed by the analysis of the spin density. It has been observed that the spin density on the Mn and on the oxo ligand can be tuned by varying the contribution of exact exchange in the functional and it is difficult to asses without a direct comparison with experiment which functional gives the most accurate description of the spin localization in the complex [37].

Table 3.1. Relative energy and important bond lengths in the di-Mn cluster 1. (a) From reference [20]. Bond lengths are given in Å and relative energies in kcal/mol. The atomic labeling refers to Figure 3.1.

multiplicity	relative energy	Mn2-O3	Mn1-O4	Mn1-O5	Mn2-O4	Mn2-O5
2	0	1.61	1.79	1.75	1.79	2.09
6	5.60	1.61	1.80	1.74	1.81	2.10
2	7.91	1.61	1.79	1.75	1.79	2.09
8	29.59	1.83	1.79	1.77	1.85	1.94
2 (a)		1.76	1.80	1.73	1.83	1.96

Additional calculations performed with the ADF program, a TZP basis set, and including dispersion corrections in different functionals give Mn-O distances close to 1.60 Å both with BLYP than with hybrid functionals (see Table 3.2). As mentioned above, this distance is usually associated more with a Mn-oxo rather than a Mn-oxyl radical. However, the Mulliken spin population analysis does not provide an

unambiguous picture for the O ligand in complex **1** since no clear trend emerges in going from standard GGA to hybrid functionals, with the BLYP-D and B3LYP*-D functionals giving -0.20 and 0.03 respectively, and OPBE0-D predicting a stronger radical character (0.67).

Table 3.2. Manganese-oxygen distances in the di-Mn complexes 1, 2 and 3. Bond lengths are given in Å. The atomic labeling refers to Figure 3.1 and 3.4.

Complex 1		
Functional	Mn2-O3	Mn1-O6
BLYP	1.62	2.16
BLYP-D	1.62	2.13
B3LYP*-D	1.60	2.10
OPBE0-D	1.54	2.11
Complex 2		
Functional	Mn1-Ox1	Mn2-Ox2
BLYP	1.60	1.62
BLYP-D	1.60	1.62
B3LYP*-D	1.57	1.57
OPBE0-D	1.55	1.53
Complex 3		
Functional	Mn-OOH	Mn-OH
BLYP	1.82	1.84
BLYP-D	1.81	1.83
B3LYP*-D	1.73	1.77

3.3.1.2 Reaction pathway analysis for complex 1

The reaction pathway involving the oxygen bond formation between one water molecule and the oxyl radical and the concerted jump of one water hydrogen to the oxo bridge is first explored, following the suggestion of Siegbahn *et al.* based on early DFT calculations [20]. A geometry optimization of complex **1**, including a water molecule initially located between the oxyl radical and one oxo-bridge, leads to a stable conformation where the water forms hydrogen bonds with both aromatic ligands. Starting from this optimized geometry, metadynamics simulation are performed with two collective variables: The distance between the water oxygen and the oxyl radical, and the distance between one water hydrogen and one oxo-bridge, assuming that the oxo bridge can act as a proton acceptor in this reaction step. The maximum value for the collective variables was set to 3Å. During this metadynamics the water hydrogen (Hw) approaches the oxo-bridge to within ~1Å distance. However, when the hydrogen reaches this configuration, the oxyl radical – water oxygen (Ox-Ow) distance is not short enough for a reaction to occur.

In a genuine solvent environment, other water molecules in the coordination sphere of the catalyst can facilitate the proton transfer step. Therefore a second water molecule is added in a position where it can act as a proton channel from the first water to the oxo-bridge.

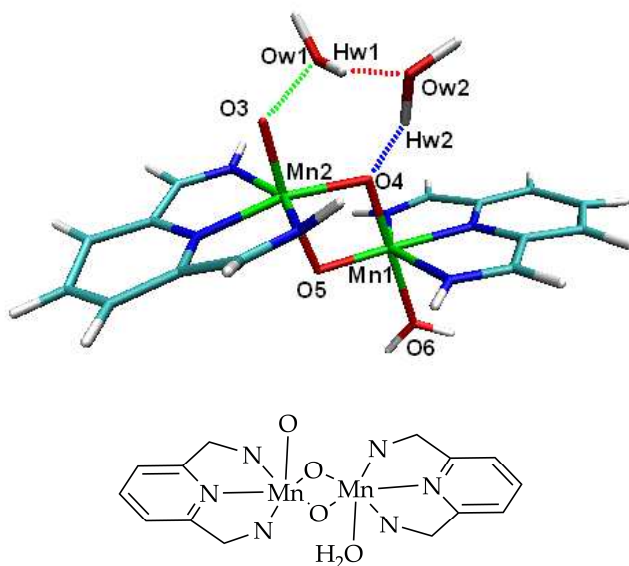


Figure 3.1. Di-manganese complex **1** with two water molecules. The dashed lines represent the collective variables used in the metadynamics simulation. The atomic labeling used throughout the paper is indicated [38].

To test if a reaction pathway is possible where the Ox-Ow bond formation is accompanied by a proton jump through the second water onto the oxo-bridge, a bias potential is included for each of the bonds expected to be formed during this reaction (see Figure **3.1**). Along this trajectory, a structural rearrangement of complex **1** takes place, as illustrated in Figure **3.2**:

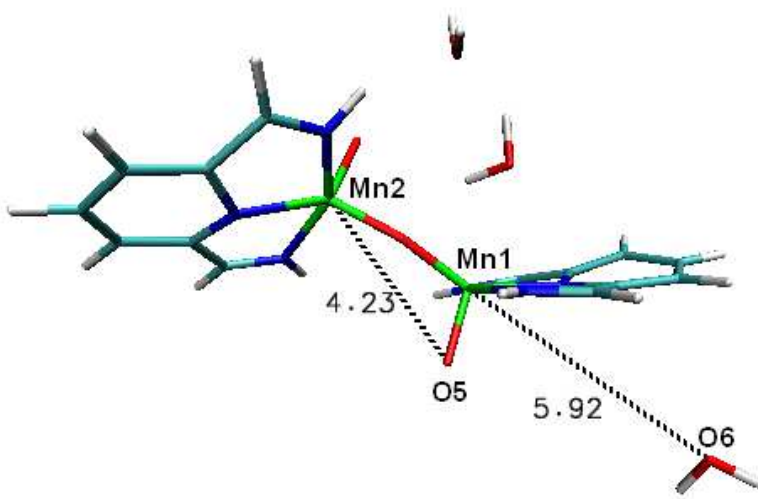


Figure 3.2. Snapshot of the di-manganese complex after 1700 MD steps. The Mn2-O5 and Mn1-O6 distances (Å) are shown to underline the structural changes observed in the simulation [38].

The aquo ligand breaks its coordination bond and at the same time one of the oxo-bridges opens up and the oxygen moves into the initial position of the aquo ligand. As a consequence of this internal rearrangement, the two manganese atoms become pentacoordinated. To verify that this structural rearrangement is not an artifact of the lack of a proper environment, this metadynamics simulation is repeated in water within the QM/MM approach (see Computational Details section). In this case however, the only collective variable is the O_x-O_w distance and all the other degrees of freedom are able to evolve freely. In this

way the proton is not forced to jump onto the oxo-bridge, which might induce the structural instability. The results are shown in Figure 3.3, where a similar structural rearrangement as observed in vacuum takes place. The opening of the oxo-bridge (orange and black lines) and the leaving of the aquo ligand (red line) occur prior to any attempt of bond formation between the oxyl radical and the oxygen water (green line), or in other words before the water oxidation process could take place. Indeed the minimum Ox-Ow distance is $\sim 2 \text{ \AA}$, in spite of the bias potential, suggesting that an activation barrier associated with the transition state is encountered at this distance.

It should be mentioned that a spin crossing might occur during a reaction involving bond splitting as discussed in Refs. [10] and [39]. Here however the structural rearrangement occurs before any sign of water splitting and therefore a different spin state in the metadynamics simulations is not considered.

In the simulations, the structural rearrangement has lower activation energy than the oxygen – oxygen bond formation. In addition, these findings underline that the oxo-bridge is not a proper proton acceptor for this catalytic reaction step. This is well in line with a theoretical study on a similar di-Ru catalyst, indicating that the hydrogen jump to the μ -oxo moiety requires a substantial structural distortion and is not thermodynamically stable [40].

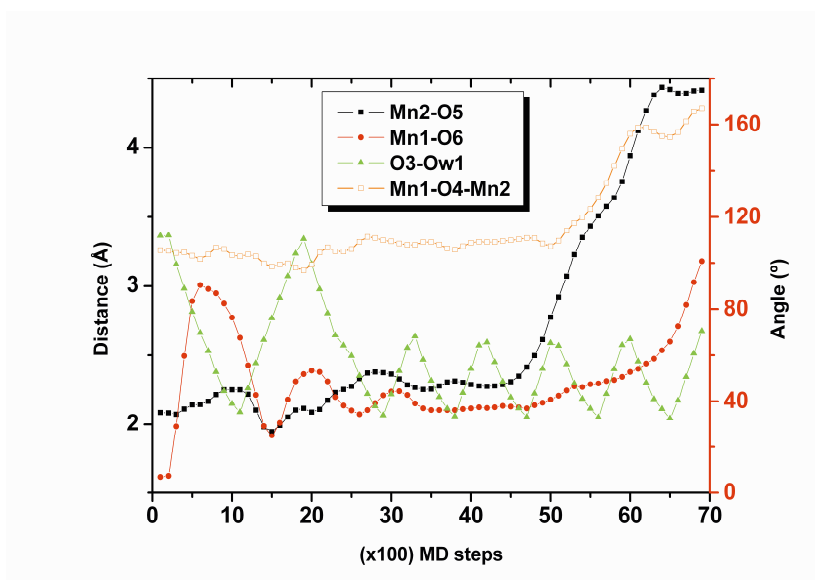


Figure 3.3. Relevant geometrical parameters during the structural rearrangement of complex 1 observed in the QM/MM simulation including the water environment.

3.3.2 Modeling of the penta-coordinated manganese cluster (2) with one oxo-bridge

3.3.2.1 Structural and electronic characterization of complex 2

A geometry optimization is performed to check the structural stability of the penta-coordinated di-Mn complex

$[(\text{bis}(\text{imino})\text{pyridine})(\text{O})\text{Mn}^{\text{IV}}(\mu\text{-O})\text{Mn}^{\text{V}}(\text{O})(\text{bis}(\text{imino})\text{pyridine})]^{3+}$ (**2**)
 obtained after the structural rearrangement of complex **1**. Also for
 complex **2** the doublet state has the lowest energy, as for complex **1**.

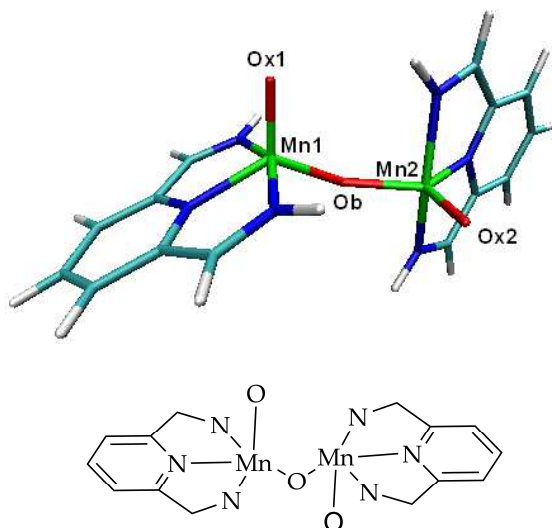


Figure 3.4. Optimized geometry of complex 2 [38]

This conclusion is warranted both in vacuum and in an explicit water environment with the quartet state being about 6 kcal/mol higher in energy. A Mulliken spin population analysis at the BLYP level gives 1.20 for Mn1 and -0.39 for Mn2. In addition, one oxo ligand shows a higher spin population (Ox1, 0.27) than the other one (Ox2, -0.10). In Table 3.2 it can be noticed that the Mn-O distances obtained with different functionals for complex **2** are very similar to those obtained

for complex **1**. The optimized geometry (see Figure **3.4**) shows a dihedral angle (θ) O_{x1}-Mn1-Mn2-O_{x2} of $\sim 90^\circ$, which could facilitate a hypothetical water oxidation path where one of the two oxo ligands can act as proton acceptor [40].

Table 3.3. Energy difference between complex 1 and complex 2 plus one water molecule [$\Delta E = E(2 + \text{water}) - E(1)$], optimized using different functionals and basis sets. STO (TZP) is a triple zeta with polarization Slater type basis set and PW (100 Ry) is a plane wave basis set with a cutoff of 100 Ry. Also the effect of empirical dispersion corrections (D), included using the Grimme parameters, is shown [31].

Basis set	Functional	ΔE (kcal/mol)
PW (100 Ry)	OPBE	-28.9
STO (TZP)	BLYP	-6.5
STO (TZP)	BLYP-D	-1.9
STO (TZP)	B3LYP	-15.1
STO (TZP)	B3LYP*-D	-13.9
STO (TZP)	OPBE0-D	-25.7

To assess whether the structural rearrangement of complex **1** is thermodynamically accessible, in Table **3.3** is shown the energy difference between complex **1** and complex **2** plus one water molecule [$\Delta E = E(2 + \text{water}) - E(1)$] for various functionals and basis sets,

including hybrid functionals and dispersion corrections. The energy comparison shows that the one oxo-bridge complex **2** is in general thermodynamically more stable than the two oxo-bridges complex **1** although the energy difference varies considerably from one functional to the other with the BLYP functional giving the smallest energy difference.

3.3.2.2 Reaction pathway analysis for complex

Having established that the complex **2** is stable and thermodynamically favorable, its potential water oxidation activity is now explored. A likely hypothetical reaction pathway involves the approach of the oxygen of a water molecule to one oxo ligand and a proton jump from the water molecule to the other oxo ligand.

Complex **2** plus a water molecule located between the two oxo ligands is considered as a starting configuration for metadynamics investigations in vacuum. During the simulation with only the Ox1-Ow distance as collective variable it is observed that as soon as the water oxygen approaches one oxo ligand ($d_{\text{Ox1-Ow}} \sim 1.6 \text{ \AA}$) the Mn1-Ox1 distance starts to increase considerably, indicating a weakening of the manganese-oxygen bond. However, the hydrogen of the water is not transferred to the other oxo ligand, and remains at a distance longer than 3 \AA . By adding a bias potential along the vector connecting a hydrogen of the approaching water with the other oxo ligand, while at the same time keeping the Ox1-Ow distance close to the bonding value,

a rapid proton transfer from the water to the other oxo ligand is observed, leading to the expected product (see Figure 3.5). This result suggests that the proton jump occurs easily when the oxygen-oxygen bond is already formed. Comparing the energy of complex **2** plus a water against the resulting [(bis(imino)pyridine)(OOH)Mn^{IV}(μ-O)Mn^V(OH)(bis(imino)pyridine)]³⁺ intermediate complex (**3**) shows that this step is endothermic.

Table 3.4. Energy difference between complex 2 plus one water molecule and complex 3 [$\Delta E = E(3) - E(2 + \text{water})$], optimized using different functionals. The first entry BLYP (PW) is the result obtained with the CPMD program using plane waves with 100 Ry cutoff. All other results are obtained with the ADF program and a triple zeta with polarization Slater type basis set (STO / TZP). The effect of empirical dispersion corrections (D) [31] is also shown. The results are presented for doublet to doublet and for a spin crossover from doublet to quartet.

Functional	$\Delta E_{\text{doublet} \rightarrow \text{doublet}}$ (kcal/mol)	$\Delta E_{\text{doublet} \rightarrow \text{quartet}}$ (kcal/mol)
BLYP (PW)	-	37.5
BLYP	24.0	33.7
BLYP-D	23.3	33.0
B3LYP-D	23.2	10.4
B3LYP*-D	21.4	12.8

In Table 3.4 the results obtained with different functionals are shown. The hybrid functionals predict a smaller energy difference than the GGA functionals and a spin crossing from a doublet to a quartet spin state.

In order to check whether the solvent environment can facilitate this reaction step by playing the role of proton acceptor [10], AIMD simulations were performed with a full QM description of the water environment (see Computational Details section). The solvate environment provides a hydrogen bonding network between various water molecules, which can allow for the proton of the reactant water molecule to jump more easily to the other oxo ligand or be solvated in the environment. Initially a metadynamics simulation was performed with a bias potential acting on the Ox1-Ow distance between the oxo ligand and the closest water. When the Ox1-Ow distance is decreasing and approaching a typical O-O bond length value of $\sim 1.4 \text{ \AA}$, the expected increase in the Mn-Ox distance is observed, as well as an increase in the internal water Hw-Ow distance. However, a complete proton transfer to the other oxyl ligand or to the water environment is never observed. This may be due to the fact that in the metadynamics simulations the evolution of the CV is quicker than the equilibration time needed by the solvent to reorganize to the current Ox1-Ow distance in order to facilitate the proton release.

For this reason additional AIMD simulations were performed without any constraint starting from the complex with the formed

hydroperoxo ligand and with the released proton relocated in the water environment. In all cases the hydroperoxo ligand appears instable, the Ox1-Ow distance increases, leading to the breakage of the bond, and the released OH⁻ reconstitutes a water molecule with the proton present in the solvent.

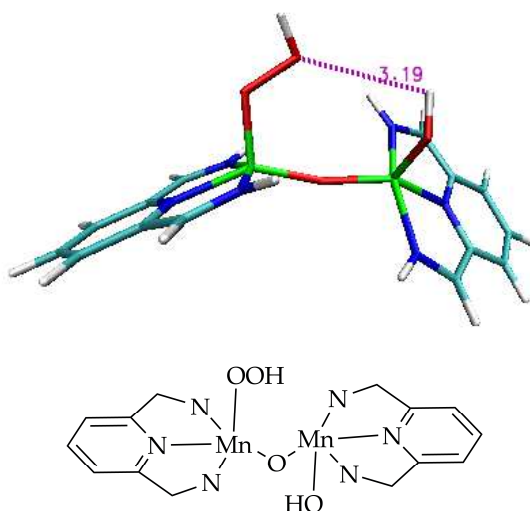


Figure 3.5. di-Mn complex intermediate after formation of the O-O bond and proton jump to the second oxyl ligand [38]. Distance between the atoms of the broken O-H bond is given in Å.

However, starting the AIMD simulation with the formed hydroperoxo ligand and with the released proton on the other oxyl ligand (as in complex **3**), the hydroperoxo ligand and the whole intermediate complex are stable in the water environment.

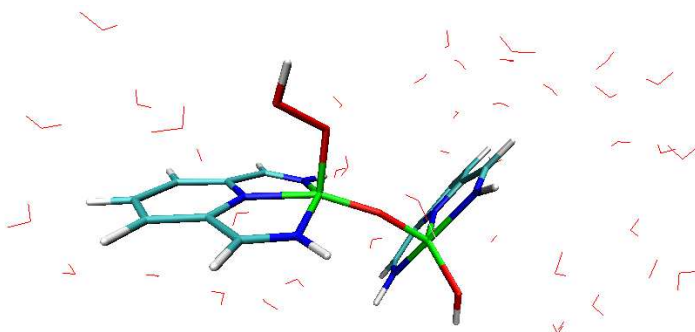


Figure 3.6. Snapshot of the stable Mn-OOH intermediate (complex **3**) taken from a AIMD simulation in fully QM water environment at room temperature without any constraint [38]

These simulations lead to the conclusion that the oxygen-oxygen bond formation step occurs only if at the same time the second oxyl ligand accepts a proton, thereby keeping the total charge of the complex unchanged. Hence complex **2** appears to be weakly active towards the formation of the O-O bond since the formation of intermediate **3** requires a thermodynamically difficult concerted reaction step.

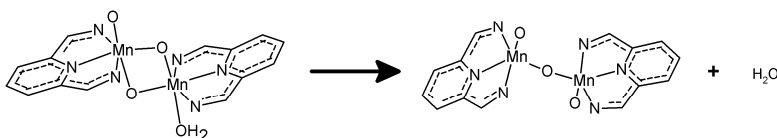
3.4 Conclusions

The search for a water oxidation catalyst based on abundant transition metals is currently an important step in the development of

artificial photosynthesis devices. Specifically Mn catalysts with oxo-bridges mimicking the natural OEC of photosystem II are being explored as possible candidates for reaching this goal. In this chapter the focus is on the reactivity of a di-Mn cluster that has been the subject of experimental and theoretical studies for more than a decade. The results are based on *ab-initio* MD simulations at room temperature, including explicitly the solvent environment, and clearly show that the cluster can easily undergo a structural rearrangement involving a breakage of one the oxo-bridges and a release of a water ligand leading to two pentacoordinated Mn sites (see Scheme 3.1). These computational results are in line with previous experimental work on this di-Mn cluster since it has been observed that the catalytic activity in aqueous solution decreases dramatically after a few cycles. [15]. It has been reported that permanganate ions or manganese oxide particles are usually the decomposition products of these Mn based catalysts. Moreover, the well known Ru based blue dimer catalyst also shows reductive cleavage of the bridging oxido ligand, similarly to the structural rearrangement proposed in this chapter [19]. It is suggested that when the two-oxo bridged cluster is in water, after a few catalytic cycles, a structural rearrangement takes place. This rearrangement leads to a complex (2) that is poorly active toward the O-O bond formation: Indeed the formation of the new oxygen-oxygen bond step requires a very specific hydrogen bonding network in order to perform a concerted proton jump to convert the second oxo ligand into an

hydroxo ligand. This can explain the decrease in the activity shown in the experimental work.

It has been pointed out that in the natural OEC the flexibility of the Mn-O-Mn angles is a key feature in facilitating the water oxidation process [5]. However in the simulations presented here, this structural flexibility in the bending of the two oxo-bridges can culminate in the opening of one of the bridges, thereby degrading the catalyst [16-18]. In the natural OEC the protein matrix in which the Mn complex is embedded provides extra stability to the catalyst, while allowing for some structural distortions to take place during the S_0 - S_4 cycle. Thus it is suggested that a proper design of the catalyst should include the design of a smart embedding matrix minimizing structural distortions leading to degradation of the catalyst, while providing the proper channels for water and proton dynamics. Anchoring the water oxidation catalyst to a nanoparticle [21], can already provide a more robust system in aqueous and oxidative conditions.



Scheme 3.1. Structural rearrangement of complex 1 to form complex 2 with a release of a water molecule in the solvent environment.

3.5 Bibliography

1. Umena, Y., Kawakami, K., Shen, J.-R., Kamiya, N., *Nature*, 473 (2011) 55-60.
2. Kok, B., Forbush, B., McGloin, M., *Photochemistry and Photobiology*, 11 (1970) 457-475.
3. Yano, J., Kern, J., Sauer, K., Latimer, M.J., Pushkar, Y., Biesiadka, J., Loll, B., Saenger, W., Messinger, J., Zouni, A., Yachandra, V.K., *Science*, 314 (2006) 821-825.
4. Britt, R.D., Campbell, K.A., Peloquin, J.M., Gilchrist, M.L., Aznar, C.P., Dicus, M.M., Robblee, J., Messinger, J., *Biochim Biophys Acta*, 1655 (2004) 158-171.
5. Siegbahn, P.E.M., *Accounts of chemical research*, 42 (2009) 1871-1880.
6. Sproviero, E.M., Gascón, J.A., McEvoy, J.P., Brudvig, G.W., Batista, V.S., *Journal of the American Chemical Society*, 130 (2008) 3428-3442.
7. Joya, K.S., Vallés-Pardo, J.L., Faheem, Y., Eisenmayer, T., Thomas, B., Buda, F., de Groot, H.J.M., *ChemPlusChem* (2012).
8. Xu, Y., Akermark, T., Gyollai, V., Zou, D., Eriksson, L., Duan, L., Zhang, R., Akermark, B., Sun, L., *Inorganic Chemistry*, 48 (2009) 2717-2719.
9. Wasylenko, D.J., Ganesamoorthy, C., Koivisto, B.D., Henderson, M.A., Berlinguette, C.P., *Inorganic Chemistry*, 49 (2010) 2202-2209.
10. Vallés-Pardo, J.L., Guijt, M.C., Iannuzzi, M., Joya, K.S., de Groot, H.J.M., Buda, F., *Chemphyschem : a European journal of chemical physics and physical chemistry*, 13 (2012) 140-146.
11. Kanan, M.W., Nocera, D.G., *Science*, 321 (2008) 1072-1075.
12. Jiao, F., Frei, H., *Angewandte Chemie International Edition*, 48 (2009) 1841-1844.

13. Wang, T., Brudvig, G.W., Batista, V.S., *Journal of chemical theory and computation*, 6 (2010) 2395-2401.
14. Ertem, M.Z., Gagliardi, L., Cramer, C.J., *Chemical Science*, 3 (2012) 1293-1299.
15. Limburg, J., Vrettos, J.S., Liable-Sands, L.M., Rheingold, A.L., Crabtree, R.H., Brudvig, G.W., *Science*, 283 (1999) 1524-1527.
16. Limburg, J., Vrettos, J.S., Chen, H., de Paula, J.C., Crabtree, R.H., Brudvig, G.W., *Journal of the American Chemical Society*, 123 (2001) 423-430.
17. Tagore, R., Chen, H., Zhang, H., Crabtree, R.H., Brudvig, G.W., *Inorganica Chimica Acta*, 360 (2007) 2983-2989.
18. Tagore, R., Chen, Crabtree, R.H., Brudvig, G.W., *Journal of the American Chemical Society*, 128 (2006) 9457-9465.
19. Limburg, B., Bouwman, E., Bonnet, S., *Coordination Chemistry Reviews*, 256 (2012) 1451-1467.
20. Lundberg, M., Blomberg, M.R.A., Siegbahn, P.E.M., *Inorganic chemistry*, 43 (2004) 264-274.
21. Li, G., Sproviero, E.M., McNamara, W.R., Snoeberger, R.C., Crabtree, R.H., Brudvig, G.W., Batista, V.S., *The journal of physical chemistry. B*, 114 (2010) 14214-14222.
22. Hatakeyama, M., Nakata, H., Wakabayashi, M., Yokojima, S., Nakamura, S., *The Journal of Physical Chemistry A*, 116 (2012) 7089-7097.
23. Laio, A., Parrinello, M., *Proceedings of the National Academy of Sciences of the United States of America*, 99 (2002) 12562-12566.
24. CPMD, <http://www.cpmd.org/>, Copyright IBM Corp 1990-2011, Copyright MPI für Festkörperforschung Stuttgart 1997-2001
25. Becke, A.D., *Physical Review A*, 38 (1988) 3098-3100.
26. Lee, C., Yang, W., Parr, R.G., *Physical Review B*, 37 (1988) 785-789.
27. Becke, A.D., *The Journal of Chemical Physics*, 98 (1993) 5648-5652.

28. te Velde, G., Bickelhaupt, F.M., Baerends, E.J., Fonseca Guerra, C., van Gisbergen, S.J.A., Snijders, J.G., Ziegler, T., *Journal of Computational Chemistry*, 22 (2001) 931-967.
29. Fonseca Guerra, C., Snijders, J.G., te Velde, G., Baerends, E.J., *Theoretical Chemistry Accounts: Theory, Computation, and Modeling (Theoretica Chimica Acta)*, 99 (1998) 391-403.
30. ADF2007.2001, SCM, Theoretical Chemistry, Vrije Universiteit, Amsterdam, The Netherlands, <http://www.scm.com/>
31. Grimme, S., *Journal of Computational Chemistry*, 27 (2006) 1787-1799.
32. Martyna, G.J., Tuckerman, M.E., *The Journal of Chemical Physics*, 110 (1999) 2810-2821.
33. Goedecker, S., Teter, M., Hutter, J., *Physical Review B*, 54 (1996).
34. Eichinger, M., Tavan, P., Hutter, J., Parrinello, M., *The Journal of Chemical Physics*, 110 (1999) 10452.
35. Laio, A., VandeVondele, J., Rothlisberger, U., *The Journal of Chemical Physics*, 116 (2002) 6941.
36. D. A. Case, T. A. Darden, T. E. Cheatham III, C. L. Simmerling, J. Wang, R. E. Duke, R. Luo, R. C. Walker, W. Zhang, K. M. Merz, B. Roberts, S. Hayik, A. Roitberg, G. Seabra, J. Swails, A. W. Goetz, I. Kolossvai, K. F. Wong, F. Paesani, J. Vanicek, R. M. Wolf, J. Liu, X. Wu, S. R. Brozell, T. Steinbrecher, H. Gohlke, Q. Cai, X. Ye, J. Wang, M.-J. Hsieh, G. Cui, D. R. Roe, D. H. Mathews, M. G. Seetin, R. Salomon-Ferrer, C. Sagui, V. Babin, T. Luchko, S. Gusarov, A. Kovalenko, and P. A. Kollman (2012), AMBER 2012, University of California, San Francisco
37. Herrmann, C., Podewitz, M., Reiher, M., *Int. J. Quantum Chem*, 109 (2009) 2430 -2446.
38. The molecular representations have been made with the program VMD owned by the Theoretical and Computational Biophysics Group, NIH Resource for Macromolecular Modeling and Bioinformatics, at the Beckman Institute,

- University of Illinois at Urbana-Champaign:
<<http://www.ks.uiuc.edu/Research/vmd/>>
39. Bernasconi, L., Belanzoni, P., Baerends, E.J., *Physical Chemistry Chemical Physics*, 13 (2011) 15272-15282.
 40. Yang, X., Baik, M.-H., *Journal of the American Chemical Society*, 128 (2006) 7476-7485.

This chapter is based on:

J.L. Vallés-Pardo, M.C. Guijt, M. Iannuzzi, K.S. Joya, H.J.M. de Groot, F. Buda,
ChemPhysChem, 13 (2012) 140-146.

Chapter 4:

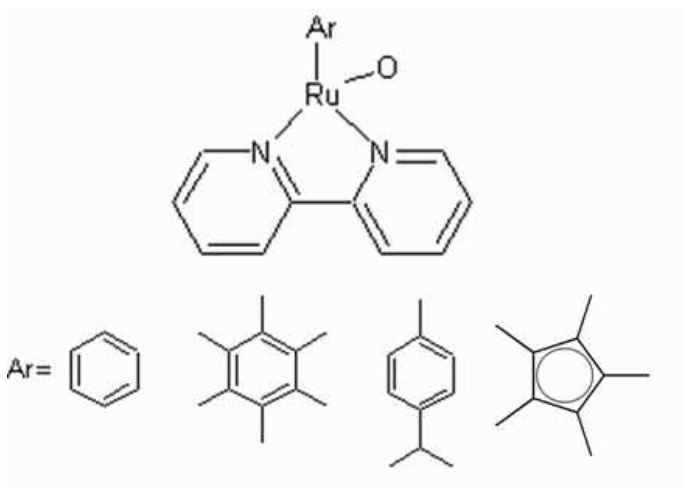
Ab-initio molecular dynamics study of water oxidation reaction pathways in mono-Ru catalysts

4.1 Introduction

One of the most important processes in natural and artificial photosynthesis is water oxidation in which water is split into O_2 and H_2 [1]. Inspired by the natural Mn based oxygen evolving complex in photosystem II, a large effort in the last decades has been devoted to synthesize transition metal complexes that can perform the same reaction. A microscopic mechanistic understanding of the natural process is clearly relevant to support the design of artificial devices for fuel generation from solar energy [2, 3]. The most successful artificial catalysts are based on Ru [4, 5], Co [2-4], and more recently Ir complexes [2]. In particular, mono-nuclear molecular catalysts based on Ir(III) have shown to be highly active and robust [10-12]. Density functional theory (DFT) calculations have been also performed to clarify the underlying reaction mechanism in some of these catalysts [10, 11, 13-15]. Available computational chemistry tools have reached a predictive power which is good enough to allow not only the understanding of reaction mechanisms in existing catalysts, but even to assist the design of new catalysts.

In this chapter the first steps in this direction are taken by performing *ab-initio* molecular dynamics (AIMD) simulations with a biasing potential [3] to study mono-Ru catalysts of the type $[(Ar)Ru(X)(bpy)]^+$. Indeed members of this class of novel mono-Ru

catalysts and closely related Ru complexes have been recently synthesized and show water oxidation activity with very high turnover numbers [4, 5]. A catalytic cycle was postulated for the Ir catalyst in Ref. [6] where the X^- ligand is initially replaced by a water molecule. This intermediate then undergoes the first two oxidation steps in which two protons and two electrons are released, yielding a formally $Ru^{IV}Oxo$ complex, which is generally assumed to be the active species in the formation of the O-O bond with another water molecule.



Scheme 4.1. Schematic drawing of the mononuclear Ru catalyst. The aromatic ligands (Ar) are, from left to right, benzene, hexamethylbenzene, cymene, and pentamethylcyclopentadienyl (Cp*)

The Ru complex and the different aromatic ligands (Ar)

considered in this chapter are shown schematically in scheme **4.1**. Here the focus is placed on this crucial reaction step starting from the Ru(IV)oxo intermediate. Possible reaction paths leading to the formation of a hydroperoxo intermediate are analyzed. Most of previous DFT based investigations on similar homogeneous catalysts are performed in the gas phase or with solvation effects included using continuum solvation models. Recent studies have underlined the importance of adding explicit water molecules since they can have a direct role in the reaction mechanism [7, 8]. In this study dynamic effects and an explicit solvent environment are included in order to provide a description of the process that is more realistic than for simulations in vacuum.

4.2 Computational details

The *ab-initio* molecular dynamics (AIMD) simulations [7] in this work are performed with the CP2K program [8]. The OPBE exchange-correlation functional for the DFT electronic structure calculations is used [9]. The choice of this non-hybrid functional is mainly dictated by the computational efficiency in the AIMD and is justified by previous work where it has been shown to give an accurate description of several transition metal complexes [15-18]. Additional tests were performed to

validate the OPBE results using the non-hybrid functional BLYP [10, 11] and the hybrid functionals B3LYP and B3LYP*, with different amounts of exact exchange, 0.2 and 0.15, respectively [11, 12]. The ADF program was used for the calculations with the hybrid functionals [13, 14]. The CP2K program employs a mixed basis set approach with Gaussian type orbitals (GTO) and plane waves (PWs) [15]. GTO functions are used to expand the molecular orbitals and the charge density in real space, whereas PWs are used for the representation of the charge density in reciprocal space. An energy cut-off of 280 Ry is used for the plane-waves basis set. The TZVP-MOLOPT-GTH [16] Gaussian basis set is chosen for all the atoms in the catalyst except ruthenium for which a DZVP-MOLOPT-GTH is used. The water molecules close to the catalyst and involved in the reaction are treated at the TZVP-MOLOPT-GTH level, whereas the DZVP-MOLOPT-GTH is used for all the other water molecules. Pseudopotentials of the GTH form for all the elements [15, 17, 18] are used. The pseudopotential for Ru is generated with 16 valence electrons. In the ADF calculations a TZP Slater type basis set is applied.

Due to the presence of π -cation interactions between the metallic centre and the aromatic ligand, it is crucial to include van der Waals corrections. In all the AIMD simulations the DFT-D2 van der Waals correction by Grimme is applied [19, 20]. Since the OPBE functional does not have its own set of correction parameters, the Grimme parameters for PBE are used instead. Periodic boundary conditions

(PBC) are applied in the simulations with explicit solvent, while for the gas phase simulations without PBC the Martina-Tuckerman approach is used for the Poisson solver [21]. For the AIMD simulations a time step $\Delta t = 0.5$ fs is considered. In order to explore possible reaction pathways, a very useful tool is the metadynamics approach proposed by Laio and Parrinello [3], which is efficiently implemented in the CP2K code. The metadynamics is a coarse-grained dynamics on the free-energy surface (FES) defined by a few collective variables (*e.g.*, the distance between two atoms) using an adaptive bias potential in order to escape from a local minimum. At each metadynamics step the evolution of the collective variables is guided by a generalized force that combines the action of the thermodynamic force, which would trap the system in a free energy minimum, and a history-dependent force that disfavors configurations already visited. This history-dependent potential is built as a sum of Gaussian functions centered in the explored values of the collective variables [3]. The height and the width of the Gaussian are 10^{-3} Hartree and 0.02 a.u., respectively. In the simulations the collective variables are evolved with one metadynamics step every 20 AIMD time steps. In this way a quick exploration of the reaction pathway can be done, at the expense of accuracy in probing the free-energy surface along the collective variable. For a preliminary estimate of the free-energy, a thermodynamic integration technique with constrained MD [22, 23] can be used instead. Six points along the Ox-Ow distance are considered in the range 1.45-2.25 Å and for each

point an equilibration of the system for about 1.5 ps is performed. This combination of the metadynamics approach and constrained MD is found to be computationally most efficient.

Simulations with explicit solvent environment are performed in an orthorhombic box of $16 \times 15.5 \times 15 \text{ \AA}^3$ containing the Ru catalyst and 73 water molecules, which are all treated at the quantum-mechanical level. Before starting the AIMD simulations, the solvent is equilibrated with force field MD simulations while keeping the transition metal complex fixed. First the volume of the box is adjusted with a constant pressure simulation and then the system is further equilibrated at constant volume and constant room temperature. For these preliminary steps the Discovery Studio software [24] is used with the CHARMM force field and the TIP3P model [25].

4.3 Results and discussion

4.3.1 Characterization of the $[(Ar)Ru(O)(bpy)]^{+2}$ intermediate

The Ru(IV)oxo complex that is assumed to be the active species in the O-O bond formation is the starting point of the investigation. The initial geometry has been generated starting from the DFT optimized coordinates of the analogous Ir based catalysts provided in Ref. [6] and

by substituting the Ir atom with Ru. The geometry of the $[(\text{Ar})\text{Ru}(\text{O})(\text{bpy})]^{2+}$ species is optimized with different aromatic ligands and for different spin states using various functionals. The inclusion of van der Waals corrections is crucial for the structural stability of the complex, as without these corrections the Ru-Ar bond breaks during the geometry optimization. Table **4.1** shows the comparison of the relative energies for different possible multiplicities. All the functionals, both hybrid and non-hybrid, give consistently the same lowest energy spin state. In particular, the triplet is the ground-state for the benzene and hexamethylbenzene ligands, while the doublet is the ground-state for the complex with the Cp* ligand. Quantitative differences between the hybrid and non-hybrid functionals, with the latter usually giving a smaller energy splitting between the two lowest states compared to the hybrid functionals, are present. Given that all functionals considered here provide consistent results, the OPBE functional was used for the subsequent AIMD simulations, because of its superior computational efficiency (see also the computational details section).

In Table **4.2** a few relevant geometrical parameters and effective RESP atomic charges [26] obtained for the most stable multiplicity using the OPBE functional are shown. These results show the effect of using different aromatic ligands on the geometric and electronic structure of the catalyst. It appears that the choice of the aromatic ring has only moderate effect on the distance between the ruthenium and the oxo ligand (Ru-O). Also the average value of the two distances between

the ruthenium and the nitrogen atoms of the bipyridine (Ru-N) are reported. The distance between ruthenium and the centre of the aromatic ring (Ru-Ar) is also an interesting parameter since a weak interaction between them could be a source of instability in the catalyst. This distance becomes shorter for increasing ring size. The effective RESP charges for ruthenium, oxygen and the aromatic ring are quite sensitive to the choice of the ligand. Specifically, the oxo ligand carries a negative charge, which increases for aromatic rings richer in electrons.

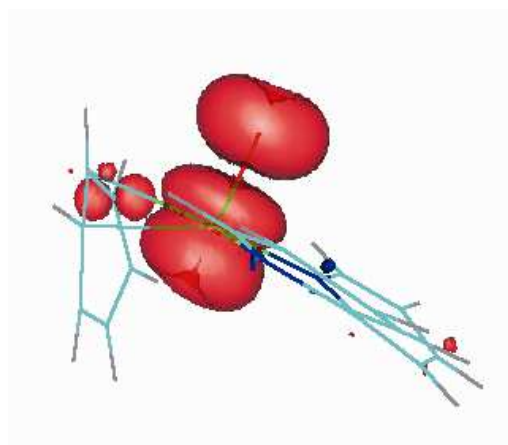


Figure 4.1. Spin density isosurface for the $[(\text{benzene})\text{Ru}(\text{O})(\text{bpy})]^{2+}$ in the triplet state. This figure has been produced with gOpenMol.

In Figure 4.1 the spin density for the $[(\text{benzene})\text{Ru}(\text{O})(\text{bpy})]^{2+}$ complex in the triplet state is shown, clearly pointing to a strong radical character of the oxo ligand, which will be indicated in the following as

the oxyl radical. This radical character has been considered a key feature to activate the O-O bond formation [27].

Table 4.1. Comparison of the energies of the [(Ar)Ru(O)(bpy)]²⁺ for different multiplicities and calculated using various functionals. The values are given in kcal mol⁻¹ and are relative to the lowest energy spin state.

Benzene				
	BLYP	OPBE	B3LYP	B3LYP*
Triplet	0	0	0	0
Singlet	3.5	6.5	13.9	13.2
Quintet	24.3	89.7	47.0	48.0

Hexamethylbenzene				
	BLYP	OPBE	B3LYP	B3LYP*
Triplet	0	0	0	0
Quintet	16.4	44.0	9.7	10.4
Singlet	224.0	7.6	20.3	19.7

Cp*				
	BLYP	OPBE	B3LYP	B3LYP*
Doublet	0	0	0	0
Quartet	22.9	22.6	29.7	29.5
Sextet	84.0	87.2	106.1	102.0

Table 4.2. Geometrical parameters and effective RESP atomic charges for the $[(\text{Ar})\text{Ru}(\text{O})(\text{bpy})]^{2+}$ complex using different aromatic rings. These results are obtained with the OPBE functional for the lowest energy spin state. Distances are given in Å, angles in degrees.

Geometrical parameters				
	Ru-O	Ru-Ar	Ru-N	O-Ru-Ar
Benzene	1.74	1.90	2.11	125.88
Hexamethylbenzene	1.73	1.80	2.25	123.87
Cp*	1.71	1.86	2.03	136.04
Effective RESP charges				
	Ru	O	Ar	
Benzene	1.86	-0.45	0.30	
Hexamethylbenzene	3.62	-1.10	0.57	
Cp*	3.45	-1.22	0.19	

4.3.2 AIMD simulations for the O-O bond formation

In this section two different reaction mechanisms for the O-O bond formation are under investigation using metadynamics simulations, as described in the computational details section. In the first scenario it is assumed that the incoming water molecule first coordinates to the Ru, thus creating a heptacoordinated intermediate, assuming that these aromatic rings are treated as tridentate ligands. This is followed by a second step in which the O-O bond could be formed. In the second case

it is considered that the incoming water molecule attacks the oxyl radical for a direct O-O reaction. These two suggested pathways are similar to those addressed in a recent theoretical study on ruthenium water oxidation catalysts [28].

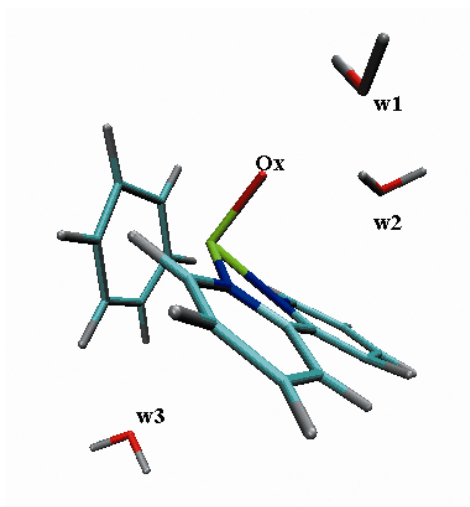


Figure 4.2. Optimized geometry of the $[(\text{benzene})\text{Ru}(\text{O})(\text{bpy})]^{2+}$ intermediate including three water molecules. This image was made with VMD [29]

In order to assess the importance of the inclusion of an extensive solvation at the quantum-mechanical level metadynamics simulations for the $[(\text{benzene})\text{Ru}(\text{O})(\text{bpy})]^{2+}$ catalyst are performed, both in vacuum and in an explicit solvent environment. For the simulations in vacuum the optimized Ru complex plus three water molecules in its proximity is taken as starting geometry (see Figure 4.2). For the simulations in the

presence of an explicit solvent environment the catalyst plus 73 water molecules are included in the molecular dynamics box with periodic boundary conditions (see also the computational details section).

4.3.2.1 Ru-Ow3 approach

In the first AIMD simulation for this approach the $[(\text{Benzene})\text{Ru}(\text{O})(\text{bpy})]^{2+}$ complex plus three water molecules are included: w1, w2 close to the oxyl radical and w3 at 3.5 Å from the Ruthenium atom on the opposite side (see Figure 4.2). The collective variable (CV) used in this simulation is the Ru-Ow3 distance with a maximum allowed value of 3.7 Å. In Figure 4.3 the Ru-Ow3 and the Ru-benzene distances along the AIMD trajectory are shown. The benzene breaks its coordination bond when the incoming water enters the coordination shell of the metal ($\text{Ru-Ow3} \approx 2.7$ Å), suggesting that this pathway is unfeasible. It should be pointed out that the biasing potential builds up also when the water is coordinated to the Ru (see Figure 4.3, after about 1 ps). This is why the water eventually leaves the Ru coordination shell in the second part of the trajectory.

In order to check if the observed structural instability of the catalyst is related to the specific choice of the aromatic ligand, or to the missing water environment, additional simulations using the same setup were performed: First the benzene ligand was substituted with hexamethylbenzene and cymene and then the same reaction path was analysed in vacuum. In addition the benzene was reconsidered in a

water solvated environment. In all these simulations a similar behaviour with the aromatic ligand leaving the coordination shell of the metal is present. In Figure 4.3 the results obtained in vacuum and in solvated environment for the benzene case are shown. The simulations reveal how the degradation of the catalyst is very similar in both cases, with the water environment only slightly slowing down the process. It can be concluded that the heptacoordinated form of the Ruthenium is not stable for this class of catalysts.

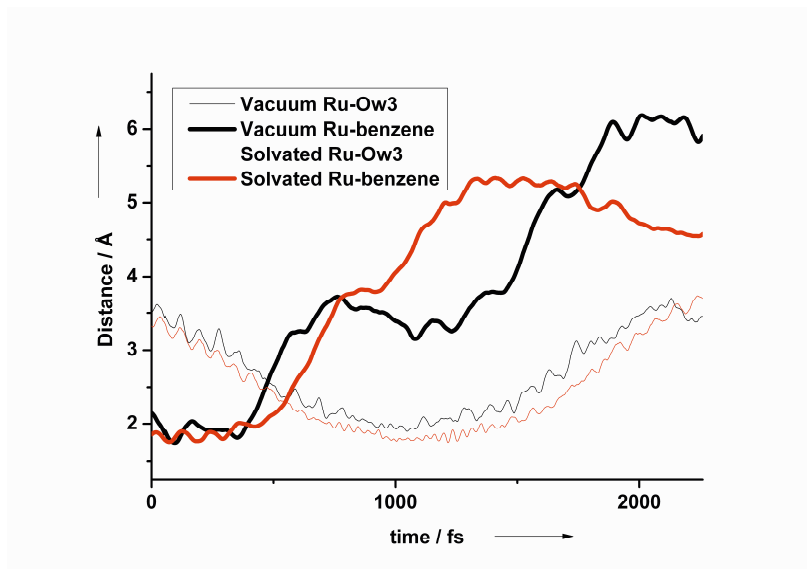


Figure 4.3. Relevant geometrical parameters along the metadynamics simulation of the $[(\text{benzene})\text{Ru}(\text{O})(\text{bpy})]^{2+}$ complex, in which the Ru-Ow3 distance is the collective variable. For the atomic labeling in the legend we refer to Figure 4.2.

4.3.2.2 Ox-Ow1 approach

The starting geometry for these metadynamics simulations is the same as used in the previous case (Figure 4.2), but here the CV is the distance between the oxyl radical and the oxygen of water w1 (Ox-Ow1) with an initial value of 3.5 Å and a maximum allowed value of 3.7 Å. When the Ox-Ow1 distance becomes less than ~ 1.8 Å, an increase of the Ru-Ox and of the Ow1-Hw1 distances occurs.

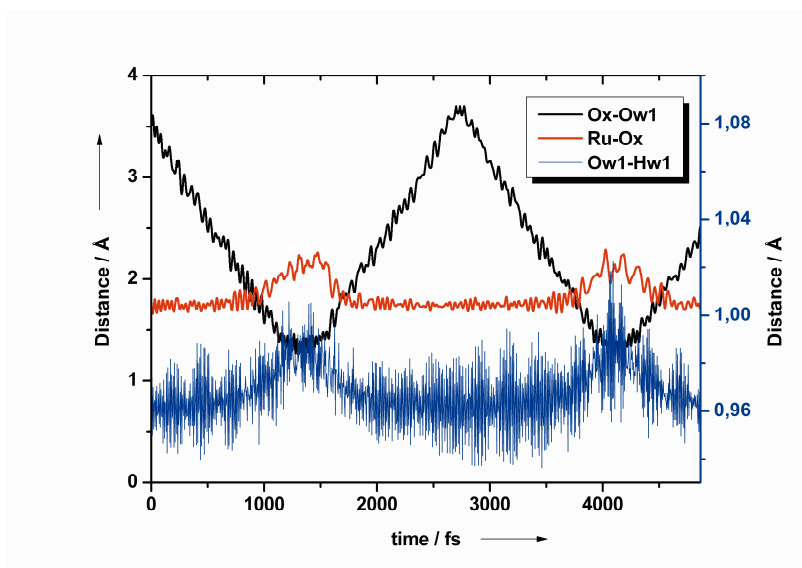


Figure 4.4. Relevant geometrical parameters along the metadynamics simulation of the $[(\text{benzene})\text{Ru}(\text{O})(\text{bpy})]^{2+}$ in the gas phase, with the Ox-Ow1 distance as the collective variable. The atomic labelling in the legend refers to Figure 4.2. The right axis refers to the Ow1-Hw1 distance (blue line).

This observation is well in line with expectations. When the bond between Ox and Ow has been established, the interaction between Ruthenium and the oxyl radical becomes weaker since the double bond character is lost. On the other hand it is also expected that the O-O bond formation would be accompanied by a proton jump from the reactant water, thus this slight increase of the Ow1-Hw1 distance can be interpreted as the initiation of a proton jump. It is clear that a proper proton acceptor in this simulation is still missing.

In order to address the question about the importance of the solvent environment for this reaction, the same metadynamics simulation in the presence of explicit water molecules surrounding the catalyst is performed (see Computational Details section). The results are illustrated in Figure 4.5, where the relevant geometrical parameters describing the reaction are plotted. It should be emphasized again that only the distance between the oxygen of the water molecule (Ow1) and the oxyl radical (Ox-Ow1, black line) is driven by the adaptive biasing potential, while all other structural changes occur spontaneously. When Ox-Ow1 is about 1.8 Å an increase in the Ru-Ox distance (red line) and an increase in the water bond length Hw1-Ow1 (blue line) can be observed, matching the result of the previously described simulation in vacuum. However, a decrease in the distance between Hw1 and the oxygen of a second water molecule (Ow2, green line) is also occurring. Soon after the Ox-Ow1 distance has reached a value of ~ 1.4 Å, indicating the formation of the O-O bond, one proton of the reactant

water jumps on the second water, thus forming a hydronium ion OH_3^+ . In Figure 4.6, a snapshot of the simulation after 1.7 ps, clearly shows the formation of the Ru-OOH intermediate and of a hydronium ion. Figure 4.5 also shows that if the metadynamics simulation continues, the biasing potential will fill the local minimum in the free energy landscape corresponding to this intermediate state and the reaction is reversed.

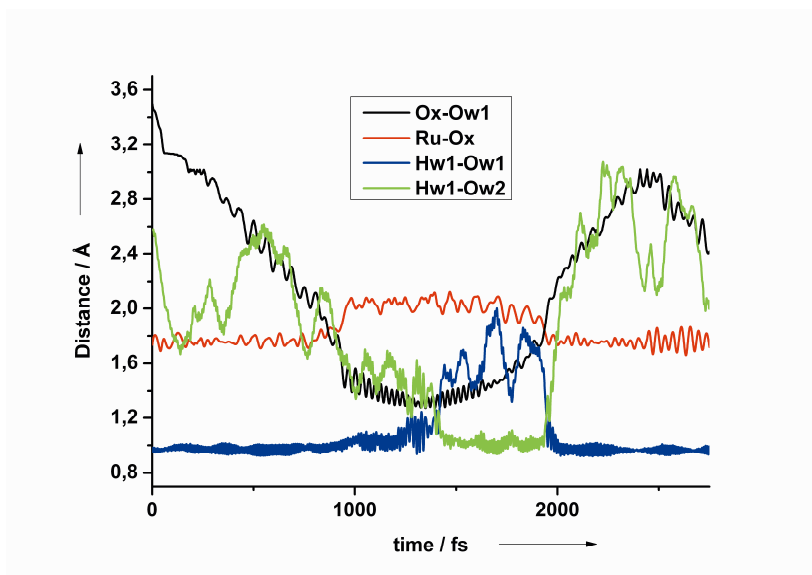


Figure 4.5. Relevant geometrical parameters along the metadynamics simulation of the solvated $[(\text{Benzene})\text{Ru}(\text{O})(\text{bpy})]^{2+}$ complex, in which the Ox-Ow1 distance is the collective variable. The atomic labelling in the legend refers to Figure 4.2

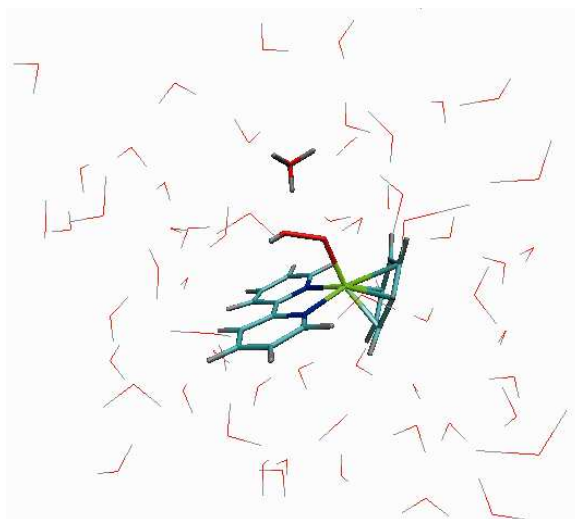


Figure 4.6. Hydroperoxo intermediate in solvated environment. The hydronium ion formed in the simulation is also highlighted. This snapshot is taken after 1.7 ps of simulation. The image was made with VMD [29]

For an estimate of the free-energy profile a thermodynamic integration technique with constrained MD is used, in which each initial configuration is extracted from the metadynamics trajectory. The preliminary estimated free-energy shows a low activation barrier of around 10 kcal mol^{-1} and a $\Delta G \approx -10 \text{ kcal mol}^{-1}$ between the Ru-OOH intermediate and the initial complex, indicating that this reaction step is exothermic. The transition state is found for an Ox-Ow1 distance between 1.85 and 1.95 Å. These constrained AIMD simulations show that the proton jumps spontaneously to the water environment when the

Ox-Ow1 distance is shorter than the transition state value. Moreover, the oxo ligand apparently never acts as a proton acceptor in the simulations, in contrast with the suggestion presented in Ref. [6]. Two additional AIMD simulations of a few ps at room temperature are also performed, without any constraints, for the solvated initial Ru-oxyl and the final Ru-hydroperoxo intermediates to verify that indeed these two intermediates are stable in water.

4.3.3 Characterization of the $[(\text{benzene})\text{Ru}(\text{OOH})(\text{bpy})]^{+1}$ intermediate and the transition state

In this section the structural and electronic properties of the Ru-OOH intermediate and the transition state found in the AIMD simulations are analyzed. In Table 4.3 a comparison between geometrical parameters and relative energies obtained in the gas phase is presented. For a proper energetic comparison, the same cubic simulation box size, with a side length of 18 Å, is considered for each supramolecular complex. Both the initial complex (Ru-oxyl) and the transition state (TS) include two water molecules, while for the hydroperoxo intermediate the hydronium cation is included. In this way each calculation has the same number of atoms and total charge.

There are a few important considerations emerging from this analysis. First, during the oxygen bond formation (Ox-Ow1) the Ru-Ox

distance increases as expected, while the Ru-benzene distance decreases. During the geometry optimization of the Ru-OOH complex with the hydronium cation, one proton is transferred from the hydronium to the Ox forming a hydrogen peroxide ligand (Ru-HOOH). This final complex resembles closely the species found for the similar Ir catalyst studied in Ref. [6]. This result is at variance with the behavior observed in the AIMD simulations in water, where the hydronium is stabilized by the solvation shell, underlining the importance of the solvent environment.

Table 4.3. Comparison between the energy in vacuum of the initial complex (Ru-oxyl) including two water molecules, the transition state (TS) and final intermediate including the hydronium (Ru-HOOH). Geometrical parameters for the hydroperoxo complex (Ru-OOH) are also reported. Distances are in Å and energies in kcal mol⁻¹. The atomic labelling refers to Figure 4.2. The lowest energy multiplicity is indicated.

	Ru-Ox	Ru-Benzene	Ox-Ow1	Relative energy	Multiplicity
Ru-oxyl	1.75	1.77	3.08	0	Triplet
TS	1.80	1.72	1.93	24.3	Singlet
Ru-HOOH	2.20	1.63	1.43	11.0	Singlet
Ru-OOH	2.00	1.63	1.43	-	Singlet

A preliminary characterization of the transition state in vacuum including the reactant water and the water accepting the proton is shown in Figure 4.7 and some of the corresponding geometrical

parameters are given in Table 4.3. In particular a $d(\text{Ox}-\text{Ow1})=1.93 \text{ \AA}$ is found and the second water (w2) is ready to accept the proton with $d(\text{Ow2}-\text{Hw1})=1.57 \text{ \AA}$. The TS energy is about 24 kcal mol^{-1} higher than for the reactant, which compares well with the value of $24.0 \text{ kcal mol}^{-1}$ found by Blakemore *et al.* for the analogous Ir catalyst when they include two water molecules [6]. However, the transition state found for the Ir complex has a distance $d(\text{Ox}-\text{Ow1})=1.50 \text{ \AA}$, which is much shorter than for our system and very close to the equilibrium O-O distance in the hydroperoxo intermediate. In fact another transition state with a similar Ox-Ow1 short distance is found, which according to the vibrational analysis corresponds to the proton transfer step from the reactant water to the second water and is not representative of the actual transition state for the O-O bond formation. From the comparison with the free-energy barrier estimated in the water environment, it could be concluded that the solvent is important in facilitating this reaction step. The energy difference between the initial and the final complex in vacuum cannot be directly compared with the result in water since two different intermediates are obtained. Therefore the results obtained with an explicit solvent are not only quantitatively but also qualitatively different from those obtained in the gas phase.

An important point that is extensively discussed in the literature for this class of catalysts is the oxidation state of the metallic centres. To check if the Ru atom increases or decreases its oxidation state during this reaction step, a RESP charge analysis of the optimized

initial (Ru-oxy) and final (Ru-OOH) intermediate states in the gas phase is performed. This analysis clearly shows that the ruthenium increases its positive charge in spite of the decrease of the overall charge of the hydroperoxo intermediate to +1. The excess positive charge on the Ru is overcompensated by an increase in the negative charge, predominantly on the benzene and in the bipyridine ligands. This increased charge polarization in the complex can explain the shortening of the Ru-benzene distance due to a stronger electrostatic interaction.

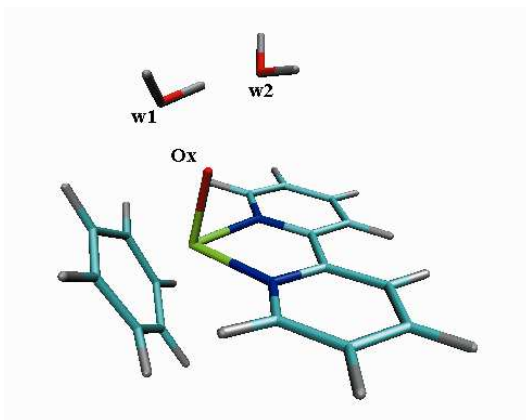


Figure 4.7. Transition state of the Ru catalyst with a benzene ligand and including two water molecules. This image was made with VMD [29]

Finally, in Table 4.3 the most stable spin multiplicity for the hydroperoxo intermediate is listed, which turns out to be a singlet,

unlike the initial complex where a triplet state was found. Therefore, the results point to the occurrence of a spin-crossover during the reaction. This spin-crossover appears to be located at (or close to) the transition state, where the singlet and triplet states differ in energy by only ~ 1 kcal mol⁻¹. This result is reminiscent of the two-state reactivity discussed by Shaik and co-workers for Fe complexes [30].

4.4 Conclusions

This chapter shows how the *ab-initio* molecular dynamics approach with an adaptive bias potential can be an important tool to efficiently explore potential reaction paths for water oxidation reactions at room temperature and with an explicit inclusion of the water environment. The focus of the analysis is a class of mononuclear ruthenium catalysts that are inspired by recently synthesized analogous iridium-based catalysts. In the computer simulations it is easy to check the effect of modifying the ligands and/or the metal centres and the predictive range of this type of *in silico* studies can assist the development of new, efficient and robust catalysts for artificial photosynthesis.

The reaction path involving first a coordination step of the reactant water to the metal centre appears unlikely since it leads to a structural

instability of the catalyst with the breaking of the metal-aromatic ligand coordination bond. The alternative path, in which the reactant water directly attacks the oxyl radical, leads to the formation of the O-O bond resulting in a Ru-hydroperoxo complex and to the release of one proton into the solvent environment. This simulation shows that the proton release occurs spontaneously at room temperature and thus is not the rate-limiting step. Moreover, it underlines the crucial role played by the solvent in facilitating the formation of the hydroperoxo intermediate with an activation free-energy of only about 10 kcal mol⁻¹. From the analysis of the charge distribution in the complex before and after the reaction, this step in the catalytic cycle can be interpreted as a proton-coupled electron transfer (PCET) process, since electron charge moves from the metallic centre to the aromatic ring. In this scheme the aromatic ligand plays the role of an electronic charge buffer, facilitating the electronic steps in the catalytic cycle. Interestingly, a spin-crossover appears to occur along this reaction path since the final intermediate is found to be a singlet while the initial Ru-oxyl complex is a triplet state. Further investigations are ongoing to get a more accurate estimate of the free energy profile and the effect of different aromatic ligands.

4.5 Bibliography

1. Lubitz, W., Reijerse, E.J., Messinger, J., *Energy & Environmental Science*, 1 (2008) 15-31.
2. McDaniel, N.D., Coughlin, F.J., Tinker, L.L., Bernhard, S., *Journal of the American Chemical Society*, 130 (2007) 210-217.
3. Laio, A., Parrinello, M., *Proceedings of the National Academy of Sciences of the United States of America*, 99 (2002) 12562-12566.
4. Joya, K.S., de Groot, H.J.M., *Metal complex and use as multielectron catalyst*, 2011, PCT/NL2011/050673
5. Bernet, L., Lalrempuia, R., Ghattas, W., Mueller-Bunz, H., Vigarà, L., Llobet, A., Albrecht, M., *Chemical Communications*, 47 (2011) 8058-8060.
6. Blakemore, J.D., Schley, N.D., Balcells, D., Hull, J.F., Olack, G.W., Incarvito, C.D., Eisenstein, O., Brudvig, G.W., Crabtree, R.H., *Journal of the American Chemical Society*, 132 (2010) 16017-16029.
7. Marx, D., Hutter, J., *Ab Initio Molecular Dynamics: Basic Theory and Advanced Methods*, Cambridge University Press, Cambridge, 2009.
8. The CP2K developers group. <http://cp2k.berlios.de/>.
9. Swart, M., Ehlers, A.W., Lammertsma, K., *Molecular Physics*, 102 (2004) 2467-2474.
10. Becke, A.D., *Physical Review A*, 38 (1988) 3098-3100.
11. Lee, C., Yang, W., Parr, R.G., *Physical Review B*, 37 (1988) 785-789.
12. Becke, A.D., *The Journal of Chemical Physics*, 98 (1993) 5648-5652.
13. te Velde, G., Bickelhaupt, F.M., Baerends, E.J., Fonseca Guerra, C., van Gisbergen, S.J.A., Snijders, J.G., Ziegler, T.,

- Journal of Computational Chemistry*, 22 (2001) 931-967.
14. ADF2007.2001, SCM, Theoretical Chemistry, Vrije Universiteit, Amsterdam, The Netherlands, <<http://www.scm.com/>>
 15. Krack, M., *Theoretical Chemistry Accounts*, 114 (2005) 145-152.
 16. VandeVondele, J., Hutter, J., *The Journal of chemical physics*, 127 (2007) 114105.
 17. Goedecker, S., Teter, M., Hutter, J., *Physical Review B*, 54 (1996).
 18. Hartwigsen, C., Goedecker, S., Hutter, J., *Physical Review B*, 58 (1998).
 19. Grimme, S., *Journal of Computational Chemistry*, 27 (2006) 1787-1799.
 20. Grimme, S., Antony, J., Ehrlich, S., Krieg, H., *The Journal of chemical physics*, 132 (2010) 154104.
 21. Martyna, G.J., Tuckerman, M.E., *The Journal of Chemical Physics*, 110 (1999) 2810-2821.
 22. Sprik, M., Ciccotti, G., *The Journal of Chemical Physics*, 109 (1998) 7737-7744.
 23. den Otter, W.K., Briels, W.J., *The Journal of Chemical Physics*, 109 (1998) 4139.
 24. Accelrys Software Inc., Discovery Studio Modeling Environment <http://accelrys.com/>.
 25. MacKerell, A.D., Bashford, D., Bellott, Dunbrack, R.L., Evanseck, J.D., Field, M.J., Fischer, S., Gao, J., Guo, H., Ha, S., Joseph-McCarthy, D., Kuchnir, L., Kuczera, K., Lau, F.T.K., Mattos, C., Michnick, S., Ngo, T., Nguyen, D.T., Prodhom, B., Reiher, W.E., Roux, B., Schlenkrich, M., Smith, J.C., Stote, R., Straub, J., Watanabe, M., WiÅ³rkiewicz-Kuczera, J., Yin, D., Karplus, M., *The Journal of Physical Chemistry B*, 102 (1998) 3586-3616.
 26. Laio, A., Gervasio, F.L., VandeVondele, J., Sulpizi, M., Rothlisberger, U., *The Journal of Physical Chemistry B*, 108 (2004) 7963-7968.

27. Lundberg, M., Blomberg, M.R.A., Siegbahn, P.E.M., *Inorganic chemistry*, 43 (2004) 264-274.
28. Wang, L.-P., Wu, Q., Van Voorhis, T., *Inorganic Chemistry*, 49 (2010) 4543-4553.
29. The molecular representations have been made with the program VMD owned by the Theoretical and Computational Biophysics Group, NIH Resource for Macromolecular Modeling and Bioinformatics, at the Beckman Institute, University of Illinois at Urbana-Champaign: <<http://www.ks.uiuc.edu/Research/vmd/>>
30. Shaik, S., de Visser, S., Ogliaro, F., Schwarz, H., Schroder, D., *Current Opinion in Chemical Biology*, 6 (2002) 556-567.

This chapter is based on:

J.L. Vallés-Pardo, H.J.M. de Groot and F. Buda. (2012). To be submitted

Chapter 5:

In silico prediction and thermodynamic study of novel mono-nuclear water oxidation catalysts

5.1 Introduction

The main goal of photosynthesis is the conversion of solar energy into chemical energy using water as source of protons and electrons. In artificial photosynthesis, using the same principles developed by nature, water can be used as a cheap and renewable material to make chemical fuels [1, 2].

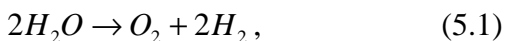
The production of hydrogen as fuel from water as raw material using sunlight is one of the most important solutions for obtaining a clean and renewable fuel source [3, 4]. One of the key and most complicated steps in building an efficient artificial photosynthetic device is the development of a robust and competent water oxidation catalyst for the generation of molecular oxygen together with the release of four protons and electrons.

During the last two decades many groups have synthesized and analyzed several water oxidation catalysts based on a variety of transition metal complexes. The review [5] is recommended for a comprehensive description of the current status in this field. The most successful artificial catalysts are based on Ru [6, 7], Co [8-10], and more recently Ir complexes [11, 12]. However, the search for a robust, efficient, and cost effective biomimetic catalytic system that can operate at optimal thermodynamic conditions is still open [8].

Computational studies, mostly based on density functional theory

(DFT) can provide a valuable complementary tool, not only to investigate reaction mechanisms, but also to evaluate and predict the free-energy diagram and reaction coordinate along the catalytic cycle. Following closely the method proposed by Nørskov and coworkers [9, 10], which has been already applied in the study of water oxidation [11] and reduction [9] on metal surfaces, a DFT study of the free-energy and overpotential for a class of mono-metallic homogenous catalysts for water oxidation is presented. The main goal is to find *in silico* trends and guiding principles for the design of optimal water oxidation catalysts. Catalysts of the type $[(\text{Ar})\text{M}(\text{H}_2\text{O})(\text{bpy})]^{n+}$, where Ar is an aromatic ring attached to the metallic center M via π -cation interaction, are investigated since they have been shown recently to be particularly promising candidates [12, 13]. The complete set of catalysts studied in this work is shown schematically in Figure 5.1.

Water oxidation is an energy intensive reaction involving the removal of four electrons and four protons. The free energy change for the conversion of two water molecules into molecular oxygen and two hydrogen molecules,



is found experimentally to be $\Delta G = 4.92$ eV at standard conditions in a pH-independent representation of the reaction coordinate.

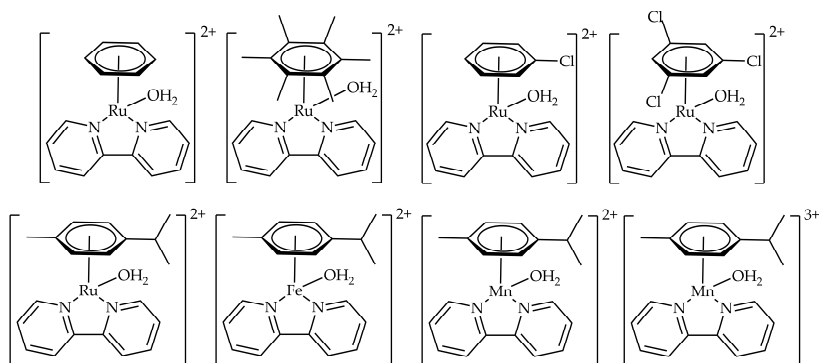
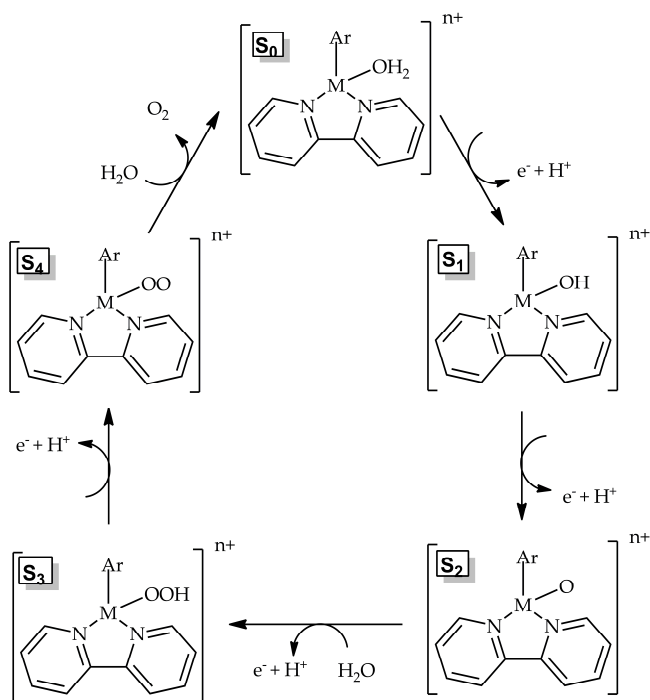


Figure 5.1. Representatives of the class of $[(Ar)M(OH_2)(bpy)]^{n+}$ monometallic molecular catalytic systems considered in this work. In the first row ruthenium catalysts with different aromatic ligands are shown. In the second row complexes with a cymene ligand and different metallic centres are presented.

The total ΔG is distributed over four steps, each ideally involving a free-energy change of 1.23 eV per electron transferred. In addition, electrolysis of water requires always some excess energy in the form of overpotential, to sustain the conversion and to prevent back reaction of the product [14]. Since the total free energy change for water oxidation is fixed at 4.92 eV, decrease of one step, below 1.23 eV, implies increase of one or more other steps, and since the largest step determines the total potential needed to drive the reaction, the variation between steps along the reaction coordinate is a good measure of the efficiency that can be obtained with a catalyst. The goal is thus to make a catalyst with a reaction coordinate that has four equal steps with the

same $\Delta G = 1.23$ eV. Scheme 5.1 shows the hypothetical catalytic cycle with four intermediates (S_0 - S_4), starting from the catalyst with a metal coordinated water molecule and ending with the oxygen molecule coordinated to the metal.



Scheme 5.1. The water splitting catalytic cycle showing the four intermediates denoted as S_1 ($M-OH$), S_2 ($M-O$), S_3 ($M-OOH$), and S_4 ($M-OO$), respectively. Each step in the cycle is assumed to be a PCET reaction. The final step involves only the ligand exchange between O_2 and H_2O .

Each intermediate is here obtained by a proton-coupled electron transfer (PCET) step. The final exchange step between oxygen and water is also shown at the end of the cycle in scheme 5.1.

5.2 Methodology and computational details

Using density functional theory (DFT) calculations it is possible to estimate the free energy differences ΔG between the intermediates in the water oxidation process for molecular catalysts with good accuracy. In this chapter the method proposed by Nørskov *et al.* [9] is followed, which has been already used for water oxidation [11] and reduction [9] on metal oxide surfaces. More methodological details can be found in the paper by Valdés *et al.* where this method has been recently applied and reviewed [15]. Here only a brief description of the important points regarding this work is given. The free energy difference ΔG is evaluated as

$$\Delta G = \Delta H + \Delta ZPE - T\Delta S, \quad (5.2)$$

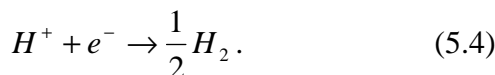
where ΔH is the enthalpy difference between the different intermediates, ΔZPE is the change in zero-point energy, which is derived from the frequencies of the vibrational normal modes through equation 5.3, both terms being calculated at the DFT level, according to

$$ZPE = \frac{1}{2} \sum_i^{3N-6} h\nu_i, \quad (5.3)$$

where N is the total number of atoms in the system.

$T\Delta S$ is the change in entropy at 300K obtained using standard thermodynamic tables for H_2O , O_2 and H_2 , provided that the changes of entropy in the catalyst are negligible compared to the other terms [10]. This assumption has been validated with an explicit calculation of the entropic term for $[(\text{cymene})\text{Ru}(\text{H}_2\text{O})(\text{bpy})]^{2+}$ shown in table **5.1**. This assumption has been used also in previous work on a polyoxometalate molecular catalyst [16].

Assuming that the catalysts work in a PCET regime, instead of computing the free-energy separately for the proton and the electron, the pair, defined by equation **5.4**, can be computed directly,



For each intermediate in the catalytic cycle (scheme **5.1**) the free-energy difference is computed according to the equations **5.5**, evaluating explicitly also the ΔG for the ligand exchange step:

$$\begin{aligned} \Delta G(S_0 \rightarrow S_1) &= G(S_1) + \frac{1}{2} G(H_2) - G(S_0), \\ \Delta G(S_1 \rightarrow S_2) &= G(S_2) + \frac{1}{2} G(H_2) - G(S_1), \end{aligned} \quad (5.5)$$

$$\Delta G(S_2 \rightarrow S_3) = G(S_3) + \frac{1}{2}G(H_2) - G(S_2) - G(H_2O),$$

$$\Delta G(S_3 \rightarrow S_4) = G(S_4) + \frac{1}{2}G(H_2) - G(S_3),$$

$$\Delta G(S_4 \rightarrow S_0) = G(S_0) + G(O_2) - G(S_4) - G(H_2O),$$

For the entropic term only the hydrogen ($TS = 0.41\text{eV}$), the water ($TS = 0.67\text{eV}$) and the oxygen ($TS = 0.64\text{eV}$) are taken into account, so the contribution for each step is as shown in equation 5.6:

$$\begin{aligned} T\Delta S(S_0 \rightarrow S_1) &= 0.205\text{eV}, \\ T\Delta S(S_1 \rightarrow S_2) &= 0.205\text{eV}, \\ T\Delta S(S_2 \rightarrow S_3) &= -0.465\text{eV}, \\ T\Delta S(S_3 \rightarrow S_4) &= 0.205\text{eV}, \\ T\Delta S(S_4 \rightarrow S_0) &= -0.03\text{eV}. \end{aligned} \tag{5.6}$$

Combining equation 5.2, 5.5 and 5.6 all the free-energy gaps for the water oxidation reaction can be calculated.

All the calculations in this work have been performed at the DFT level [17] using the QuickStep method [18] included in the CP2K software [19]. This code employs a mixed basis set approach with Gaussian-type orbitals (GTO) and plane-waves (PWs). GTO functions are used to expand the molecular orbitals and the charge density in real space, whereas PWs are used for the representation of the charge

Table 5.1. Energetic parameters (including enthalpy) including solvent model (COSMO). The values of ΔE , ΔZPE , $T\Delta S$, and ΔG are obtained following the equation 5.5 in the main text.

	$E(\text{eV})$	$TS(300\text{K})(\text{eV})$	$ZPE(\text{eV})$	$\Delta E(\text{eV})$	$\Delta ZPE(\text{eV})$	$T\Delta S(\text{eV})$	$\Delta G(\text{eV})$
S_0	-291.93	1.78	10.57	0			
S_1	-286.73	1.80	10.24	1.84	-0.19	0.22	1.43
S_2	-281.89	1.74	9.95	1.50	-0.16	0.15	1.20
S_3	-291.48	1.84	10.34	1.43	-0.03	-0.29	1.68
S_4	-287.05	1.77	10.07	1.08	-0.13	0.13	0.81
S_4-S_0				-0.17	0.04	0.03	-0.16
Total							4.96
Water	-14.37	0.59	0.55				
H_2	-6.70	0.41	0.27				
O_2	-9.65	0.61	0.09				

density in reciprocal space. An energy cut-off of 280 Ry is used for the plane-waves basis set. The TZVP-MOLOPT-GTH [20] Gaussian basis set is chosen for all the atoms in the catalyst except the metallic centers for which a DZVP-MOLOPT-GTH is used.

The OPBE [21] exchange-correlation functional is used for the DFT electronic structure calculations. The choice of this non-hybrid functional is mainly due to previous works where it has been shown to give an accurate description of several transition metal complexes [22, 23], and is also supported by previous comparison with different functionals (BLYP, B3LYP, B3LYP* [24-26]) in a group of catalysts of the same family as those treated in this chapter [13].

For all the elements, pseudopotentials of the GTH form are used [27-29]. The pseudopotentials of the metallic atoms are generated assuming as valence electrons those that belong to the two highest main quantum numbers.

Van der Waals corrections are included for a proper description of the π -cation interaction between the metallic center and the aromatic ligand. Specifically the DFT-D2 correction by Grimme is applied [30, 31], assuming the same parameters as for the PBE functional. All the calculations are performed in vacuum in a cubic box of 18 Å per side, using the Martina-Tuckerman approach [32] for the Poisson solver. For coherence and for a proper comparison the same computational setup is used for all different catalysts studied, both for the geometrical optimization and the vibrational analysis.

Additional test calculations have been performed with the ADF code [33], using a Slater type orbital triple zeta polarized basis set (STO-TZP).

5.3 Results and discussion

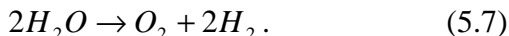
This study focuses on water oxidation catalysts of the type $[(\text{Ar})\text{M}(\text{H}_2\text{O})(\text{bpy})]^{n+}$, also shown in previous work [12, 13]. First the results about the influence of the aromatic ring using ruthenium as metallic center will be presented. Then the metallic center will be modified using the aromatic ring that shows the best performance in the previous part.

For each different metal the most stable multiplicity in each step is analyzed with the OPBE functional and is shown in Table 5.2.

Table 5.2. Lowest energy multiplicities for different metallic centres catalysts in each intermediate.

	Ru	Fe	Mn(II)	Mn(III)
S0	singlet	quintet	sextet	quintet
S1	doublet	sextet	quintet	quartet
S2	triplet	quintet	quartet	triplet
S3	doublet	doublet	quintet	quartet
S4	triplet	triplet	quartet	triplet

As a first step the accuracy of the DFT setup used in this work and the assumptions made in the methodology are checked by calculating the overall free energy change in the hydrolysis reaction (equation 5.7).



Following the procedure explained in the previous section a total reaction free-energy of 4.30 eV is obtained in vacuum. This is 0.62 eV less than the experimental result. In previous work the total free-energy change was fixed at the experimental value to avoid the explicit calculations of O_2 , since it was claimed that this is not accurately described with DFT [10]. Here it is found that the main source of error is in the use of a vacuum environment, since a test calculation including water solvent effects in a continuous model (COSMO) [34] already provides a much better agreement with experiment (see Table 5.1 and Figure 5.2).

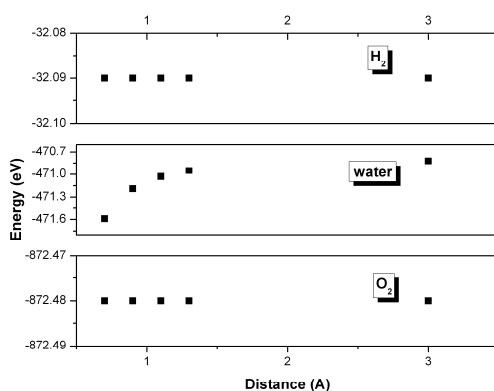


Figure 5.2. Energy for water, hydrogen and oxygen using different distances to the spherical solvent boundary.

In particular the enthalpy of the water molecule is very sensitive to the inclusion of the COSMO model, with a solvation energy that can be as large as ~ 0.3 eV per water molecule, while there is little effect on the ΔH for the hydrogen and oxygen molecules (see Figure 5.2). Therefore in order to reproduce the total free-energy change of 4.92 eV, a correction of 0.31 eV for the enthalpy term of each water molecule is included in equation 5.5 to compensate for the missing solvation effect. In addition, the solvation effects are similar for the various intermediates, since the total charge and the number of hydrogen bonds between the catalyst and the water environment are constant and therefore they cancel in the ΔG .

5.3.1. Influence of the aromatic ligand

While usually the metal atom is considered the most important part of a monometallic catalyst, the aromatic ligand can also play a crucial role in defining the electronic structure of the transition metal complex. In particular, the aromatic ring can act as an electron buffer during the catalytic cycle [13]. The rings used in this research are benzene, cymene, hexamethylbenzene, chlorobenzene and 1,3,5-trichlorobenzene, attached to a ruthenium metallic center that has shown a good performance in electroassisted water oxidation catalysis [35, 36]. The five catalysts are schematically described in Figure 5.1.

In Figure 5.3 two representations of ΔG along the reaction coordinate at 0V (Figure 5.3a) and at the equilibrium potential of

1.23eV (Figure 5.3b) are shown for the different catalytic steps S_0 - S_4 (see scheme 5.1). The optimal case where in each step the free-energy gap is 1.23 eV is also shown.

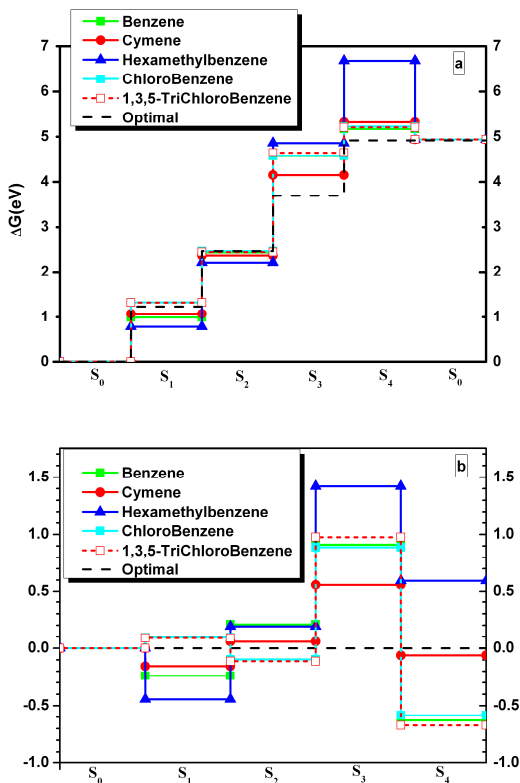


Figure 5.3. Plot of ΔG in $[(Ar)Ru(H_2O)(bpy)]^{2+}$ for different aromatic ligands. Optimal case also represented. a) at 0V. b) at 1.23V

The S_2 - S_3 step corresponds with the largest free-energy gap, which is usually observed also experimentally. The molecular complex shows the best thermodynamic overpotential of 0.56 eV with the cymene as aromatic ring. This number compares quite well with the experimentally determined overpotential of ~ 0.6 [37]. In contrast, according to the modeling hexamethylbenzene is not a good choice as aromatic ring for water oxidation, indicating that a strong electron-donor ligand is not favorable for this reaction. Cymene appears to be the best compromise between a strong electron acceptor ligand (as chlorobenzene or 1,3,5-trichlorobenzene) and a strong electron-donor ligand (as hexamethylbenzene).

In order to resolve common denominators in the reaction coordinates for the five different catalysts, the evolution of three relevant geometrical parameters, the Ru-O, averaged Ru-N, and Ru-Ar distances of the various intermediates in the catalytic cycle are shown in Figure 5.4.

The Ru-O distances show a common trend with a decrease from S_0 to S_2 and a subsequent increase from S_2 to S_4 . This corresponds with an increase of bond character from the Ru-aquo to the Ru-oxyl intermediate and a subsequent decrease until the oxygen molecule is formed and released.

The change in the bond length is associated to a clear change in the frequency of vibrational modes localized on the Ru-O moiety. The

distance between the ruthenium and the aromatic ring has the opposite behaviour, showing that the ring is more than a simple spectator and participates in the reaction by concerted motion that is correlated with the variation of the Ru-O motif. On the other hand, the distance to the bipyridine is almost constant along the reaction coordinate, corresponding to some experimental results in previous work, where it has been shown that changes in the bipyridine type ligand have little effect on the free energy plot of the catalytic reaction [37].

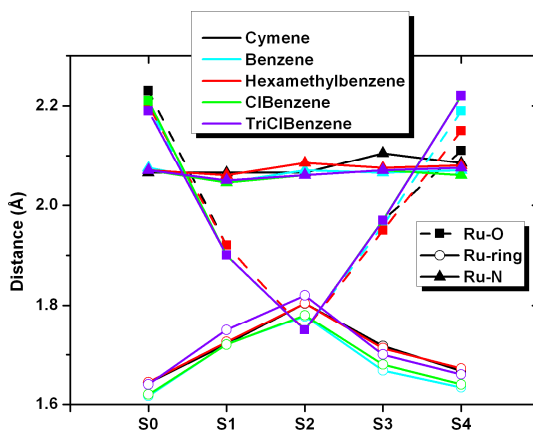


Figure 5.4. Relevant geometrical parameters for describing the reaction coordinate along the catalytic cycle.

5.3.2. Influence of the metallic center

While the $[(\text{cymene})\text{Ru}(\text{H}_2\text{O})(\text{bpy})]^{2+}$ shows the best performance among the various aromatic ligands that were investigated, ruthenium is

scarce and difficult to apply in terrestrial applications of energy conversion by water oxidation. The simulation method allows for a screening of more abundant elements as metallic catalytic centers in cymene-based molecular complexes, and simulations have been performed for iron, and manganese (Figure 5.1). Although iridium is known to be a good mono-nuclear water oxidation catalyst, it is not included in this analysis since it is known experimentally that it functions in a non-PCET regime [12].

The manganese can adopt different oxidation states. A good catalyst operation can be expected for Mn with an overall charge of +2 or +3 for the complex. In Figure 5.5 the free-energy plot for each intermediate is shown at 0V (Figure 5.5a) and at 1.23 eV (Figure 5.5b).

The $[(\text{cymene})\text{Mn}(\text{H}_2\text{O})(\text{bpy})]^{3+}$ complex shows very good performance with only slightly higher overpotential of 0.59 eV compared with the Ru benchmark.

In Figure 5.6 the same geometrical parameters as in Figure 5.4 for the various representatives of this class of catalysts are shown. In the comparison between different metallic centers the metal-oxygen distance and the metal-nitrogen distance follow similar trends as shown above in Figure 5.4. The metal-oxygen distance (Figure 5.6c) decreases between the S_0 - S_2 steps and then increases again until the S_4 step, while the metal-nitrogen distance (Figure 5.6b) remains almost constant along the whole catalytic cycle. However the distances between the metallic center and the cymene (Figure 5.6a), due to π -cation interactions, are

very sensitive to the metal atom used in the catalyst. There is no clear trend as it was the case for different aromatic ligands.

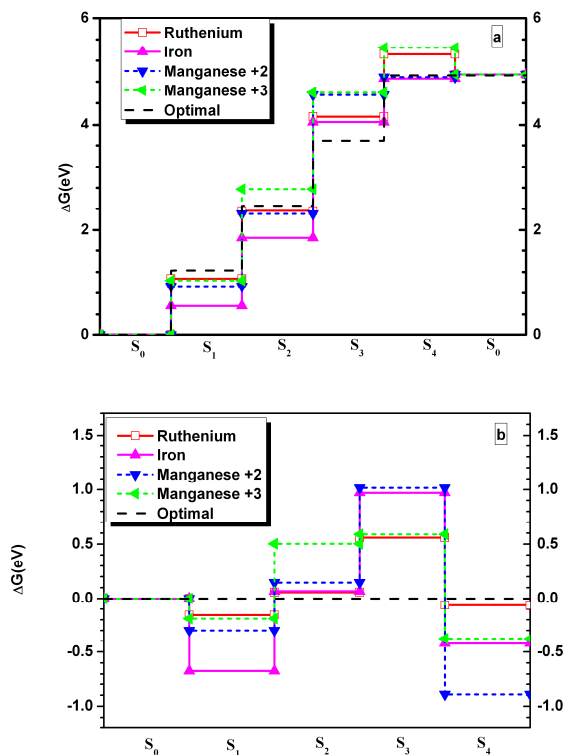


Figure 5.5. Plot of ΔG in $[(\text{cymene})\text{M}(\text{H}_2\text{O})(\text{bpy})]^{n+}$ for different metallic centres. Optimal case is also represented. a) at 0V. b) at 1.23V

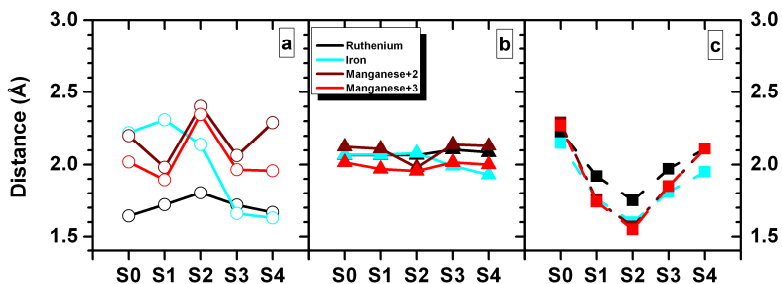


Figure 5.6. Relevant geometrical parameters along the catalytic cycle. a) M-cymene b) M-nitrogen c) M-oxygen

5.4 Conclusions

The search for an efficient water oxidation catalyst is an important step in the development of artificial photosynthesis devices. The available efficient $[(\text{cymene})\text{Ru}(\text{OH}_2)(\text{bpy})]^{2+}$ catalyst represents a good starting point for computational studies on other members of the same class, in particular those with abundant transition metals with perspective for future large scale application.

For the study of this branch of catalysts one of the most important points in the procedure is that all steps, the four PCET and the ligand exchange, are calculated explicitly. The systematic error in the total free-energy change through the whole cycle is traced back primarily to

the missing solvent effect for the water molecules, instead of limitations in the DFT for the oxygen molecule, as was assumed in earlier work. Consequently, a specific solvent correction for the H₂O molecule is sufficient to allow for a more accurate analysis of all the intermediate steps.

The computational results for the [(cymene)Ru(OH₂)(bpy)]²⁺ catalyst are in a good agreement with the free-energy obtained experimentally [37]. This validates the procedure used in this work. The ruthenium catalyst with the cymene ligand shows the lowest overpotential among all the analyzed catalysts. Interestingly, also the [(cymene)Mn(OH₂)(bpy)]³⁺ turns out to be a good catalyst as well, with an overpotential only 0.03 eV larger than in the Ru case. Since manganese is more abundant than ruthenium by about six orders of magnitude, it is worth to consider this Mn complex as a potential candidate for water oxidation.

Another important point in the *in silico* development of suitable water oxidation catalysts is the identification of possible geometrical trends that allow a better understanding of the role and importance of the different ligands. Most probably the bipyridine ligand is important only for anchoring the metal ion and does not play an active role in the catalytic cycle, since the distance to the metallic center is almost the same in all reaction intermediates across the different members of the [(Ar)M(OH₂)(bpy)]ⁿ⁺ class. The distance between the metallic center and the oxygen is changing along the cycle following the change in the

bond character as one would expect. This behaviour is common to all analyzed catalysts. The weak π -cation interaction between the aromatic ring and the metal atom is very sensitive to the metal involved. The relative distance between the aromatic ligand and the metal is changing considerably along the cycle, although it is possible to identify a trend only for catalyst with different aromatic rings, but not for different metals.

5.5 Bibliography

1. Lewis, N.S., *Nature*, 414 (2001) 589-590.
2. Meyer, T.J., *Nature*, 451 (2008) 778-779.
3. Schlapbach, L., *Nature*, 460 (2009) 809-811.
4. Najafpour, M.M., Ehrenberg, T., Wiechen, M., Kurz, P., *Angewandte Chemie International Edition*, 49 2233-2237.
5. Joya, K.S., Vallés-Pardo, J.L., Faheem, Y., Eisenmayer, T., Thomas, B., Buda, F., de Groot, H.J.M., *ChemPlusChem* (2012).
6. Xu, Y., Akermark, T., Gyollai, V., Zou, D., Eriksson, L., Duan, L., Zhang, R., Akermark, B., Sun, L., *Inorganic Chemistry*, 48 (2009) 2717-2719.
7. Wasylenko, D.J., Ganesamoorthy, C., Koivisto, B.D., Henderson, M.A., Berlinguette, C.P., *Inorganic Chemistry*, 49 (2010) 2202-2209.
8. Koper, M.T.M., *Journal of Electroanalytical Chemistry*, 660 (2011) 254-260.
9. Nørskov, J.K., Rossmeisl, J., Logadottir, A., Lindqvist, L., Kitchin, J.R., Bligaard, T., Jónsson, H., *The Journal of Physical Chemistry B*, 108 (2004) 17886-17892.
10. Rossmeisl, J., Logadottir, A., Nørskov, J.K., *Chemical Physics*, 319 (2005) 178-184.
11. Rossmeisl, J., Qu, Z.W., Zhu, H., Kroes, G.J., Nørskov, J.K., *Journal of Electroanalytical Chemistry*, 607 (2007) 83-89.
12. Hull, J.F., Balcells, D., Blakemore, J.D., Incarvito, C.D., Eisenstein, O., Brudvig, G.W., Crabtree, R.H., *Journal of the American Chemical Society*, 131 (2009) 8730-8731.
13. Vallés-Pardo, J.L., Guijt, M.C., Iannuzzi, M., Joya, K.S., de Groot, H.J.M., Buda, F., *Chemphyschem : a European journal of chemical physics and physical chemistry*, 13 (2012) 140-146.

14. Rossmeisl, J., Dimitrievski, K., Siegbahn, P., Norskov, J.K., *Journal of Physical Chemistry C*, 111 (2007) 18821-18823.
15. Valdés, A., Kroes, G.J., *The Journal of Physical Chemistry C*, 114 (2010) 1701-1708.
16. Piccinin, S., Fabris, S., *Physical Chemistry Chemical Physics*, 13 (2011) 7666-7674.
17. Parr, R.G., Yang, W., *Density-Functional Theory of Atoms and Molecules* Oxford University Press, 1989.
18. VandeVondele, J., Krack, M., Mohamed, F., Parrinello, M., Chassaing, T., Hutter, J., *Computer Physics Communications*, 167 (2005) 103-128.
19. The CP2K developers group. <http://cp2k.berlios.de/>.
20. VandeVondele, J., Hutter, J., *The Journal of chemical physics*, 127 (2007) 114105.
21. Swart, M., Ehlers, A.W., Lammertsma, K., *Molecular Physics*, 102 (2004) 2467-2474.
22. Groenhof, A.R., Ehlers, A.W., Lammertsma, K., *Journal of the American Chemical Society*, 129 (2007) 6204-6209.
23. Liao, M.-S., Watts, J.D., Huang, M.-J., *The Journal of Physical Chemistry A*, 111 (2007) 5927-5935.
24. Becke, A.D., *Physical Review A*, 38 (1988) 3098-3100.
25. Lee, C., Yang, W., Parr, R.G., *Physical Review B*, 37 (1988) 785-789.
26. Becke, A.D., *The Journal of Chemical Physics*, 98 (1993) 5648-5652.
27. Goedecker, S., Teter, M., Hutter, J., *Physical Review B*, 54 (1996).
28. Hartwigsen, C., Goedecker, S., Hutter, J., *Physical Review B*, 58 (1998).
29. Krack, M., *Theoretical Chemistry Accounts*, 114 (2005) 145-152.
30. Grimme, S., *Journal of Computational Chemistry*, 27 (2006) 1787-1799.

31. Grimme, S., Antony, J., Ehrlich, S., Krieg, H., *The Journal of chemical physics*, 132 (2010) 154104.
32. Martyna, G.J., Tuckerman, M.E., *The Journal of Chemical Physics*, 110 (1999) 2810-2821.
33. ADF2007.2001, SCM, Theoretical Chemistry, Vrije Universiteit, Amsterdam, The Netherlands, <http://www.scm.com/>
34. Klamt, A., Schuurmann, G., *Journal of the Chemical Society, Perkin Transactions 2* (1993) 799-805.
35. Bernet, L., Lalrempuia, R., Ghattas, W., Mueller-Bunz, H., Vigara, L., Llobet, A., Albrecht, M., *Chemical Communications*, 47 (2011) 8058-8060.
36. K.S.Joya, Groot, H.J.M.d., *Metal complex and use as multielectron catalyst*, 2011, PCT/NL2011/050673
37. K.S.Joya, *Molecular catalytic system for efficient water splitting*, Universiteit Leiden, 2011

Chapter 6:

General Discussion and Outlook

Chapter 6

General Discussion and Outlook

In this thesis different catalysts for the water oxidation reaction have been studied. In chapter **5** a thermodynamic study for single-metal catalysts with similar coordinating ligands was performed, obtaining a free energy profile along the whole PCET catalytic cycle. This study allows to evaluate *in silico* the overpotential for each catalyst and to identify structural and/or electronic features that minimize the overpotential, thus providing guiding principles in selecting a promising candidate as WOC.

In chapter **3** and **4** a mechanistic study of the oxygen-oxygen bond formation in the S₂-S₃ step of the catalytic cycle has been performed for

a di-Mn complex and for a mono-nuclear ruthenium catalyst, respectively. From this dynamical study useful information about the reaction mechanism, kinetics and activation barriers can be obtained. Moreover these AIMD simulations can be performed in the presence of an explicit water environment.

Ideally one would like to combine the thermodynamic study with the dynamical simulation of the different reaction steps in the catalytic cycle. This is still challenging for several reasons: Due to the nature of the PCET reaction, in which half hydrogen molecule is released in each step, the number of electrons in the metal complex and therefore its multiplicity is changing along the reaction path. Moreover, one should include in the simulation box also a chemical agent (e.g. Ce^{IV}) able to change its oxidation state to facilitate the electron transfer coupled to the proton transfer.

The possibility of simulating the reaction pathways from the dynamical studies taking into account the proper electronic structure changes along the catalytic cycle will be a very important step in the complete understanding of the whole water oxidation reaction.

The first steps in this direction have been already undertaken during the last months of this thesis project and should constitute a natural follow-up of this research. By performing constrained molecular dynamics (CMD) simulations for different fixed values of the reaction coordinate, one can monitor more extensively each stage of the reaction, checking for example also the ground state multiplicity at

each value of the constraint. Then, the average lagrangian multiplier obtained for each simulation, which represents the constraint force, can be used to derive the free-energy profile through thermodynamic integration. In this way it is also possible to better characterize the transition state and to establish the onset of the PCET step.

Another important question to address in future research is what happens when the catalyst is coupled to a charge separator module in an artificial photosynthesis device. In particular, it is crucial to assess how the electronic structure of the catalyst is affected by different charge separator complexes.

SAMENVATTING

Een van de belangrijkste processen voor het voortbestaan van het leven op aarde is fotosynthese. In dit proces wordt zonlicht, met gebruik van water en kooldioxide, omgezet in chemische energie en opgeslagen als koolhydraten. Het nabootsen van de wateroxidatiereactie in een kunstmatig apparaat, zodat zonlicht kan worden omgezet naar milieuvriendelijke brandstoffen, wordt beschouwd als een van de belangrijkste uitdagingen voor het oplossen van de huidige globale energie- en milieuproblemen. Het is om deze reden dat er in de laatste paar decennia meer onderzoek gedaan wordt naar het splitsen van water. In de eerste pogingen probeerde de wetenschappelijke gemeenschap het natuurlijke zuurstofproducerende complex (oftewel de oxygen evolving complex, OEC) van photosystem II te begrijpen en reproduceren, gebruikmakend van gelijkwaardige structuren en metaal atomen. Na verloop van tijd werd gebruik gemaakt van andere metalen, evenals complexen met minder dan vier metallische centra. Vandaag de dag is de kennis van het proces sterk verbeterd en is het mogelijk om mono-nucleaire katalysatoren te vinden, terwijl een breed scala aan atomen gebruikt kan worden als metallisch centrum. In mijn proefschrift laat ik de bijdrage van verscheidene

computationele methodes zien, die het inzicht in het proces verbeteren en de ontwikkeling van nieuwe katalysatoren die de wateroxidatiereactie optimaliseren bevorderen.

In het inleidende hoofdstuk wordt een brede kijk op het fotosynthetisch proces gegeven, met nadruk op de rol van het OEC. Verder wordt relevante literatuur over artificiële fotosynthese en verschillende wateroxidatie katalysatoren samengevat. In hoofdstuk **2** wordt de theoretische achtergrond van alle methoden die in dit proefschrift gebruikt worden besproken.

De volgende twee hoofdstukken bevatten een gedetailleerd onderzoek naar twee verschillende klassen van katalysatoren. In hoofdstuk **3** wordt een di-mangaan katalysator onderzocht die enkele jaren geleden werd voorgesteld door Limburg *et al.* Dit onderzoek maakt gebruik van een aantal van de meest avanceerde moleculaire dynamica methodes om een diep begrip van de katalyse mechanisme te ver krijgen. Een structurele verschuiving, die plaats vindt vóór de formatie van de verwachte zuurstof-zuurstof binding, leidt naar een intermediair complex, waarin de twee metallische centra door maar één zuurstofbrug verbonden worden. Het blijkt mogelijk voor dit tijdelijk complex om de wateroxidatiereactie te katalyseren. Verder wordt een mogelijk mechanisme met deze nieuwe intermediair gepresenteerd, waarin het tweede oxyl radicaal als proton acceptor optreedt, wat de formatie van de zuurstof-zuurstof binding mogelijk maakt. Vervolgens wordt in hoofdstuk **4** de katalysator $[(\text{benzeen})\text{Ru}(\text{O})(\text{bpy})]^{2+}$

geanalyseerd. Twee mogelijke reactiemechanismen zijn onderzocht. Op basis van de *in silico* studies kan worden geconcludeerd dat het reactiemechanisme dat verloopt via een interne herschikking, waarin het inkomende watermolecuul eerst een ligand van het metallische centrum wordt (hierbij een hepta-gecoördineerd intermediair vormend) en vervolgens de nieuwe zuurstof-zuurstof binding gecreëerd wordt, niet geschikt is. In plaats daarvan is de directe reactie, die tussen het oxo-ligand en het reagerende watermolecuul, het meest waarschijnlijk voor deze katalysator. Dit hoofdstuk laat ook zien dat het expliciet definiëren van een oplosmiddel omgeving in de simulaties nodig is om het reactiemechanisme te reproduceren, en om nauwkeurige overgangstoestanden te krijgen.

In hoofdstuk 5 wordt dezelfde klasse van katalysatoren gebruikt als in hoofdstuk 4. Nu wordt een thermodynamisch onderzoek gedaan. Vanuit deze berekeningen wordt het vrije energie profiel voor de hele katalyse cyclus en de overpotential voor elke katalysator gesimuleerd. Deze overpotential wordt gebruikt als een parameter om de prestaties van de katalysator te meten. Vanuit dit onderzoek kan worden geconcludeerd dat $[(\text{cymene})\text{Ru}(\text{OH}_2)(\text{bpy})]^{2+}$ de beste wateroxidatiekatalysator in deze klasse is, op de voet gevolgd door $[(\text{cymene})\text{Mn}(\text{OH}_2)(\text{bpy})]^{3+}$. Deze tweede biedt mogelijkheden om gebruikt te worden in een “kunstmatig blad” omdat Mn in grote hoeveelheden op aarde beschikbaar is.

Ten slotte wordt in hoofdstuk **6** een kort toekomstperspectief gegeven, waarin de resterende vragen worden toegelicht en mogelijke manieren om het onderzoek verder voort te zetten uitgelegd worden.

SUMMARY

One of the key processes for sustaining life on earth is photosynthesis. In this process the sunlight, using water and carbon dioxide as raw materials, is converted into chemical energy and stored as carbohydrates. Mimicking the water oxidation reaction in an artificial device in order to be able to convert the sunlight in carbon-neutral fuels is considered one of the most important challenges for solving the world-wide energy and environmental problems. For this reason during the last decades the scientific effort on water splitting has been growing. During the first attempts the scientific community tried to understand and reproduce properly the natural oxygen evolving complex (OEC) of photosystem II, using the same kind of structure and metallic atoms. Over time other metals started to be used, as well as complexes with less than four metallic centers. Nowadays the knowledge of the process is much improved and it is possible to find mono-nuclear catalysts, while a broad range of atoms can be used as metallic centers. In my thesis I show the contribution of various computational methods for gaining understanding of the process and in

the development of new catalysts to optimize the water oxidation reaction.

In the introductory chapter a broad perspective on the photosynthetic process, emphasizing the role of the OEC, is presented. Also relevant literature information about the artificial devices and the different water oxidation catalysts is summarized. Then, in chapter 2, the theoretical background of all methods used in this thesis is discussed.

The next two chapters contain a detailed study of the reaction pathways for two different classes of catalysts. In chapter 3 a dimanganese catalyst presented several years ago by Limburg *et al.* is studied. This work is performed with some of the most advanced molecular dynamics tools in order to obtain profound understanding of the catalysis mechanism. It is shown how a structural rearrangement, which takes place before the expected oxygen-oxygen bond formation, leads to an intermediate complex in which the two metallic centers are linked only by one oxygen bridge. This transient complex appears to be able to catalyze the water oxidation reaction. Also the possible mechanism involving this newly discovered intermediate is presented, pointing to the second oxyl radical as the proton acceptor that mediates the oxygen-oxygen bond formation reaction. Next, in chapter 4, the catalyst analyzed is the $[(\text{benzene})\text{Ru}(\text{O})(\text{bpy})]^{2+}$. Two different possible reaction pathways are investigated. Based on the *in silico* studies it can be concluded that the pathway in which the incoming

water molecule first becomes a ligand of the metallic center, leading to a heptacoordinated intermediate, is not suitable. Instead the direct reaction between the oxo-ligand and the reactant water molecule is the most appropriate for this catalyst. This chapter also shows that including an explicit solvent environment in the simulations is crucial to reproduce properly the reaction pathway and the intermediates.

In chapter 5, the same family of catalysts as in chapter 4 is used. This time a thermodynamic study is performed. From these calculations the free-energy profile for the whole catalytic cycle and the overpotential are obtained for each catalyst. This overpotential can be of use as it is one of the parameters that measures the performance of the catalyst. From this study it could be concluded that $[(\text{cymene})\text{Ru}(\text{OH}_2)(\text{bpy})]^{2+}$ represents the best option among the water oxidation catalysts of this class, followed closely by the $[(\text{cymene})\text{Mn}(\text{OH}_2)(\text{bpy})]^{3+}$. The second one, may be a very promising candidate for being part of an “artificial leaf”, due to the large earth abundance of the Mn metal.

Finally, in chapter 6, a brief future perspective about the remaining open questions and the possible methodology that could be used for going deeper into the research is given.

RESUM

Un dels processos claus per al manteniment de la vida al planeta és la fotosíntesi. En aquest procés la llum solar és convertida, emprant aigua i diòxid de carboni com matèria prima, en energia química i emmagatzemada com carbohidrats. Imitar la reacció d'oxidació de l'aigua en un dispositiu artificial per poder convertir la llum solar en combustibles lliures de carboni és considerat un dels reptes més importants per solucionar el problema energètic i mediambiental que pateix el planeta. Per aquest motiu, durant les darreres dècades, els esforços en la reacció d'escissió de la molècula d'aigua han anat en augment. Durant les primeres etapes la comunitat científica va intentar comprendre i reproduir adientment el complex d'evolució d'oxigen (OEC, de l'anglès Oxygen Evolving Complex) al fotosistema II, emprant el mateix tipus d'àtoms metàl·lics i el mateix tipus d'estructura. Amb el temps començaren a emprar-se altres metalls, de la mateixa forma que complexes amb menys de quatre centres metàl·lics. Avui en dia el coneixement del procés és molt major, sent possible trobar catalitzadors mono-nuclears, a més d'un ampli ventall

d'àtoms com a centres metàl·lics. A la meua tesis mostre la contribució de diferents mètodes computacionals en l'augment del coneixement del procés i el desenvolupament de nous catalitzadors per optimitzar la reacció d'oxidació de l'aigua.

Al capítol introductori s'exposa una ampla perspectiva al voltant del procés fotosintètic, fent èmfasi al paper del OEC. També es presenta la bibliografia més rellevant al voltant dels diferents catalitzadors i dispositius artificials existents. Després, al capítol **2**, s'explica la base teòrica de tots els mètodes emprats en la tesis.

Els següents dos capítols contenen un estudi detallat dels camins de reacció per a dos tipus diferents de catalitzadors. Al capítol **3** s'estudia un catalitzador amb dos àtoms de manganés presentat temps enrere per Limburg *et al.* Aquest treball és portat a terme amb algunes de les ferramentes més avançades de dinàmiques moleculars amb la intenció d'obtenir un coneixement més detallat del mecanisme de catàlisi. Es mostra com una reestructuració, que té lloc abans de la formació de l'enllaç d'oxigen, arribant a un intermedi de reacció en el qual els dos centres metàl·lics es troben lligats a soles per un pont d'oxigen, Aquest complex de transició pareix ser capaç de catalitzar la reacció d'oxidació de l'aigua. El possible mecanisme que involucra aquest recentment descobert intermedi és també presentat, apuntant al segon radical oxil com l'acceptor de protons necessari per portar a terme la formació de l'enllaç oxigen-oxigen. Per altre costat, al capítol **4**, el catalitzador analitzat és el $[(\text{benzè})\text{Ru}(\text{O})(\text{bpy})]^{2+}$. En aquest, dos

possibles camins de reacció són investigats. Basant-nos en els estudis computacionals es pot concloure que la ruta en la qual la molècula d'aigua entrant es coordina primer al centre metàl·lic, obtenint un intermedi heptacoordinat, no és l'adient. En canvi, la reacció directa entre el lligant oxo i la molècula d'aigua involucrada en la reacció és la convenient per a aquest catalitzador. En aquest capítol també es mostra que la inclusió explícita en les simulacions d'un medi aquós és crucial per a reproduir adientment el camí de reacció i els seus intermedis.

Al capítol 5, partint de la mateixa família de catalitzadors que al capítol 4 es porta a terme en aquesta ocasió un estudi termodinàmic. Mitjançant aquestes simulacions s'obté el perfil d'energia lliure del cicle catalític complet i el sobrepotencial per a cada ú dels diferents catalitzadors analitzats. Aquest sobrepotencial pot ser emprat per a mesurar el rendiment del catalitzador. Seguint aquest estudi es pot concloure que el $[(\text{cymene})\text{Ru}(\text{OH}_2)(\text{bpy})]^{2+}$ representa la millor opció entre els catalitzadors analitzats, tenint molt a prop el $[(\text{cymene})\text{Mn}(\text{OH}_2)(\text{bpy})]^{3+}$. Aquest últim pot ser considerat un candidat molt prometedor per a formar part d'una "fulla artificial" degut a la gran quantitat de manganès que hi ha al planeta.

Finalment, al capítol 6, es mostra una xicoteta perspectiva de futur al voltant de les qüestions que continuen obertes, així com els possibles mètodes que podrien ser emprats per a aprofundir en la seva comprensió.

RESUMEN

Uno de los procesos clave para el mantenimiento de la vida en el planeta es la fotosíntesis. En este proceso la luz solar es convertida, usando agua y dióxido de carbono como materias primas, en energía química y almacenada como carbohidratos. Imitar la reacción de oxidación del agua en un dispositivo artificial para poder convertir la luz solar en combustibles libres de carbono es considerado uno de los retos más importantes para solucionar el problema energético y medioambiental que sufre el planeta. Por este motivo, durante las últimas décadas los esfuerzos en la reacción de ruptura de la molécula de agua han ido en aumento. Durante las primeras etapas la comunidad científica intentó entender y reproducir adecuadamente el complejo de evolución del oxígeno (OEC, del inglés Oxygen Evolving Complex) en el fotosistema II, empleando el mismo tipo de átomos metálicos y el mismo tipo de estructura. Con el tiempo se empezaron a usar otros metales, al igual que complejos con menos de cuatro centros metálicos. Hoy en día el conocimiento del proceso es mucho mayor, siendo posible encontrar catalizadores mono-nucleares, además de un amplio

abanico de átomos como centros metálicos. En mi tesis muestro la contribución de varios métodos computacionales en el incremento del conocimiento del proceso y en el desarrollo de nuevos catalizadores para optimizar la reacción de oxidación del agua.

En el capítulo introductorio se expone una amplia perspectiva del proceso fotosintético, haciendo hincapié en el papel del OEC. También se presenta la bibliografía más relevante sobre los diferentes catalizadores existentes y los dispositivos artificiales. Luego, en el capítulo **2**, se explica la base teórica de todos los métodos usados en la tesis.

Los siguientes dos capítulos contienen un estudio detallado de los caminos de reacción para dos tipos diferentes de catalizadores. En el capítulo **3** se estudia un catalizador con dos átomos de manganeso presentado tiempo atrás por Limburg *et al.* Este trabajo es llevado a cabo con algunas de las herramientas más avanzadas de dinámicas moleculares con intención de obtener un conocimiento más profundo del mecanismo de catálisis. Se muestra como una reestructuración, la cual tiene lugar antes de la formación del enlace de oxígeno, conduce a un intermedio de reacción en el cual los dos centros metálicos se encuentran unidos por solo un puente de oxígeno. Este complejo de transición parece ser capaz de catalizar la reacción de oxidación del agua. El posible mecanismo que envuelve este recién descubierto intermedio es también presentado, apuntando al segundo radical oxyll como el aceptor de protones necesario para llevar a cabo la formación

del enlace oxígeno-oxígeno. Por otro lado, en el capítulo 4, el catalizador analizado es el [(benceno)Ru(O)(bpy)]²⁺. En este, dos posibles caminos de reacción son investigados. Basándonos en los estudios computacionales se puede concluir que la ruta en la cual la molécula de agua entrante se coordina primero al centro metálico, obteniendo un intermedio heptacoordinado, no es la adecuada. En cambio, la reacción directa entre el ligando oxo y la molécula de agua involucrada en la reacción es la apropiada para este catalizador. En este capítulo también se muestra que la inclusión explícita en las simulaciones de un medio acuoso es crucial para reproducir adecuadamente el camino de reacción y sus intermedios.

En el capítulo 5, se parte de la misma familia de catalizadores que en el capítulo 4, llevando a cabo en esta ocasión un estudio termodinámico. A través de estas simulaciones se obtiene el perfil de energía libre del ciclo catalítico completo y el sobrepotencial para cada uno de los diferentes catalizadores analizados. Este sobrepotencial puede ser útil como parámetro para medir el rendimiento del catalizador. A través de este estudio se puede concluir que el [(cymene)Ru(OH₂)(bpy)]²⁺ representa la mejor opción entre los catalizadores analizados, seguido muy de cerca por el [(cymene)Mn(OH₂)(bpy)]³⁺. Este último puede ser considerado un candidato muy prometedor para formar parte de una “hoja artificial” debido a la gran cantidad de manganeso presente en el planeta.

Finalmente, en el capítulo **6**, se muestra una pequeña perspectiva de futuro sobre las cuestiones que permanecen abiertas, así como los posibles métodos que pueden ser usados para profundizar en su comprensión.

CURRICULUM VITAE

From September 2003 until June 2008 I was a Chemistry student at the *Universitat de València*, joining during the last year the BOC-SSNMR group at Universiteit Leiden as an Erasmus student. The subject of my master work was: “*Study of a synthetic manganese catalyst for water splitting*”. During this year I participated in the Honours Class “*From Solar to Fuel with Bio*”.

After receiving my Master in Chemistry in September 2008, I started my PhD at the Universiteit Leiden under the supervision of Dr. Francesco Buda and Prof. Huub de Groot. During my PhD I participated in different schools and workshops, including *Theoretical Chemistry and Spectroscopy* (Han-sur-Lesse, Belgium, 2008), *Solar Biofuels from Microorganisms* (Leiden, 2009), *The Artificial Leaf* (Leiden, 2010), *Modeling Natural and Artificial Photosynthesis* (Leiden, 2011) and *The Artificial leaf* (Twente, 2012). In 2010 I have been also visiting for a period of two weeks the Physikalisch Chemisches Institut in Zürich, where I worked in the department of

Prof. Dr. Jürg Hutter learning from the developers the basics of the CP2K software. I presented my research work at various meetings and conferences, with poster presentations at *MolSim: Understanding Molecular Simulation* (Amsterdam, 2010), *Psi-K* (Berlin, 2010), *Modeling Natural and Artificial Photosynthesis* (Leiden, 2011) and *CPMD Meeting* (Barcelona, 2010); and with oral presentations at *CHAINS* (Maarsen, The Netherlands, 2011) and *HRSMC meeting* (Amsterdam, 2012).

LIST OF PUBLICATIONS

- **“Ab-initio molecular dynamics study of water oxidation reaction pathways in mono-Ru catalysts”**

J.L. Vallés-Pardo, M.C. Guijt, M. Iannuzzi, K.S. Joya, H.J.M. de Groot, F. Buda, *ChemPhysChem: a European journal of chemical physics and physical chemistry* 13 (2012) 140-146.

- **“Structural rearrangements and reaction intermediates in a di-Mn water oxidation catalyst”**

J.L. Vallés-Pardo, H.J.M. de Groot and F. Buda, *Physical Chemistry Chemical Physics*, 14 (2012) 15502-15508.

- **“Molecular Catalytic Assemblies for Electro-driven Water Splitting”**

K.S. Joya, J.L. Vallés-Pardo, Y. Faheem, T. Eisenmayer, B. Thomas, F. Buda, H.J.M. de Groot, *ChemPlusChem* (2012). DOI: 10.1002/cplu.201200161. *Accepted*.

- **“*In silico* prediction and thermodynamic study of novel mononuclear water oxidation catalysts”**

J.L. Vallés-Pardo, H.J.M. de Groot and F. Buda. (2012). *To be submitted.*

